

1 **Reconstructing past hydrology of eastern Canadian boreal catchments using clastic**  
2 **varved sediments and hydro-climatic modelling: 160 years of fluvial inflows**

3

4

5 Antoine Gagnon-Poiré<sup>1-2-3</sup>, Pierre Brigode<sup>4</sup>, Pierre Francus<sup>1-2-3-5</sup>, David Fortin<sup>1-6</sup>, Patrick  
6 Lajeunesse<sup>7</sup>, Hugues Dorion<sup>7</sup> and Annie-Pier Trottier<sup>7</sup>

7

8 <sup>1</sup> *Institut national de la recherche scientifique, Centre Eau Terre Environnement, Québec,*  
9 *QC, Canada.*

10 <sup>2</sup> *GEOTOP, Research Centre on the Dynamics of the Earth System, Montréal, QC,*  
11 *Canada.*

12 <sup>3</sup> *Centre d'études nordiques, Québec, QC, Canada.*

13 <sup>4</sup> *Université Côte d'Azur, CNRS, OCA, IRD, Géoazur, Nice, France.*

14 <sup>5</sup> *Canada Research Chair in Environmental sedimentology.*

15 <sup>6</sup> *Department of Geography and Planning, University of Saskatchewan, Saskatoon, SK,*  
16 *Canada.*

17 <sup>7</sup> *Département de géographie, Université Laval, Québec, QC, Canada.*

18

19 Corresponding author: Antoine Gagnon-Poiré ([Antoine.Gagnon-Poire@ete.inrs.ca](mailto:Antoine.Gagnon-Poire@ete.inrs.ca))

20 **Abstract**

21 Analysis of short sediment cores collected in Grand Lake, Labrador, revealed that this lake  
22 is an excellent candidate for the preservation of laminated sediments record. The great  
23 depth of Grand Lake, the availability of fine sediments along its tributaries, and its  
24 important seasonal river inflow have favoured the formation of a 160 years-long clastic  
25 varved sequence. Each varve represents one hydrological year. Varve formation is mainly  
26 related to spring discharge conditions with contributions from summer and autumn rainfall  
27 events. The statistically significant relation between varve parameters and the Naskaupi  
28 River discharge observations provided the opportunity to develop local hydrological  
29 reconstructions beyond the instrumental period. The combined detrital layer thickness and  
30 the particle size (99th percentile) series extracted from each varve yield the strongest  
31 correlations with instrumental data ( $r = 0.68$  and  $0.75$ ) and have been used to reconstruct  
32 Naskaupi River mean and maximum annual discharges, respectively, over the 1856-2016  
33 period. The reconstructed Q-mean series suggest that high Q-mean years occurred during  
34 the 1920-1960 period and a slight decrease in Q-mean takes place during the second half  
35 of the 20<sup>th</sup> century. Independent reconstructions based on rainfall-runoff modelling of the  
36 watershed from historical reanalysis of global geopotential height fields display a  
37 significant correlation with the reconstructed Naskaupi River discharge based on varve  
38 physical parameters. The Grand Lake varved sequence contains a regional hydrological  
39 signal, as suggested by the statistically significant relation between the combined detrital  
40 layer thickness series and the observed Labrador region Q-mean series extracted from five  
41 watersheds of different sizes.

Supprimé: minor

Supprimé: hydroclimatic

42  
43 **1. Introduction**

44 Climate changes caused by rising concentrations of greenhouse gases can alter hydro-  
45 climatic conditions on inter- and intra-regional scales (Linderholm et al., 2018; Ljungqvist  
46 et al., 2016; Stocker et al., 2013). Hydropower, which is considered as a key renewable  
47 energy source to mitigate global warming, has strong sensitivity to changes in hydrological  
48 regime especially in vulnerable northern regions (Cherry et al., 2017). Therefore, a clear  
49 understanding of the regional impacts that recent climate change combined with natural  
50 climate variability can have on river discharge and hydroelectric production is needed.

53 However, the lack of instrumental records and the uncertainty related to hydroclimate  
54 variability projections (Collins et al., 2013) are obstacles to sustainable management of  
55 these water resources.

56

57 The Labrador region in eastern Canada is a critical area for hydropower generation, hosting  
58 the Churchill River hydroelectric project, one of the largest hydropower systems in the  
59 world. Average annual streamflow has been varying in eastern Canada during the last fifty  
60 years, with higher river discharges from 1970 to 1979 and 1990 to 2007, and lower  
61 discharges from 1980 to 1989 (Mortsch et al., 2015; Déry et al., 2009; Jandhyala et al.,  
62 2009; Sveinsson et al., 2008; Zhang et al. 2001). These changes in streamflow represent a  
63 significant economic challenge for the long-term management of hydropower generation.  
64 The few decades of available instrumental observations (<60 years) and their low spatial  
65 coverage are not sufficient to allow a robust analysis of multi-decadal hydrological  
66 variability.

67

68 The study of multi-decadal hydrological variability requires long instrumental records  
69 (>100 years), but such long-time series are non-existent for the Labrador region. Recently,  
70 rainfall-runoff modelling approaches have been used to expand instrumental streamflow  
71 datasets, using long-term climatic reanalysis as inputs. Rainfall-runoff modelling was used  
72 by Brigode et al. (2016) to reconstruct daily streamflow series over the 1881–2011 period  
73 in northern Québec. Nevertheless, this type of method suffers from the limited observations  
74 in order to evaluate and validate the reconstructed hydro-climatic temporal series. The  
75 deficiency of observations led to the exploration of various natural archives for  
76 reconstructing past hydro-climatic conditions. Long hydro-climatic series based on natural  
77 proxies in eastern Canada are rare, limited to a tree ring (Boucher et al., 2017; Begin et al.,  
78 2015; Naulier et al., 2015; Nicault et al., 2014; Boucher et al., 2011; Begin et al., 2007;  
79 D'Arrigo et al., 2003) and pollen datasets (Viau et al., 2009) and mainly focused on  
80 temperature reconstructions. Reconstructing river hydrological series using dendrological  
81 analysis is complex in the boreal region due to the indirect relation between tree ring  
82 indicators and streamflow. One study has reconstructed streamflow variations over the last  
83 two centuries in Labrador based on tree-ring isotopes series (Dinis et al., 2019). Still, the

84 spatial coverage of palaeohydrological records from independent proxies must be increased  
85 in this region. In this perspective, annually laminated sediments composed of minerogenic  
86 particles (clastic varves) formed when seasonal runoff carrying suspended sediment enters  
87 a lake (Sturm, 1979) have the potential to produce long paleohydrological series. The direct  
88 relationship between clastic varves and hydrological conditions makes this type of varve a  
89 specific and powerful proxy for streamflow reconstructions. Clastic varves can provide, in  
90 favourable settings, annually to seasonally resolved information about downstream  
91 sediment transport from catchment area into lake basin depending on regional hydro-  
92 climatic conditions (Lamoureux, 2000; Lamoureux et al., 2006; Tomkins et al., 2010;  
93 Cuvén et al., 2011; Kaufman et al., 2011; Schillereff et al., 2014; Amann et al., 2015;  
94 Heideman et al., 2015; Zolitschka et al., 2015; Saarni et al., 2016; Czymzik et al., 2018).

95

96 Preliminary analysis of short sediment cores collected in Grand Lake, central Labrador,  
97 revealed that this lake is an excellent candidate for the preservation of recent fluvial clastic  
98 laminated sediment record (Zolitschka et al., 2015). The objectives of this paper are to: (1)  
99 Confirm the annual character of the laminations record; (2) Establish the relation between  
100 the physical parameters of laminations and local hydrological conditions to examine the  
101 potential proxy for hydrological reconstructions; (3) Reconstruct the hydrology of the last  
102 160 years and compare its similarities and differences with Brigode et al. (2016) rainfall-  
103 runoff modelling over the 1880-2011 period; and (4) Determine if there is a Labrador  
104 regional streamflow signal recorded in Grand Lake laminated sediments.

105

## 106 **2. Regional setting**

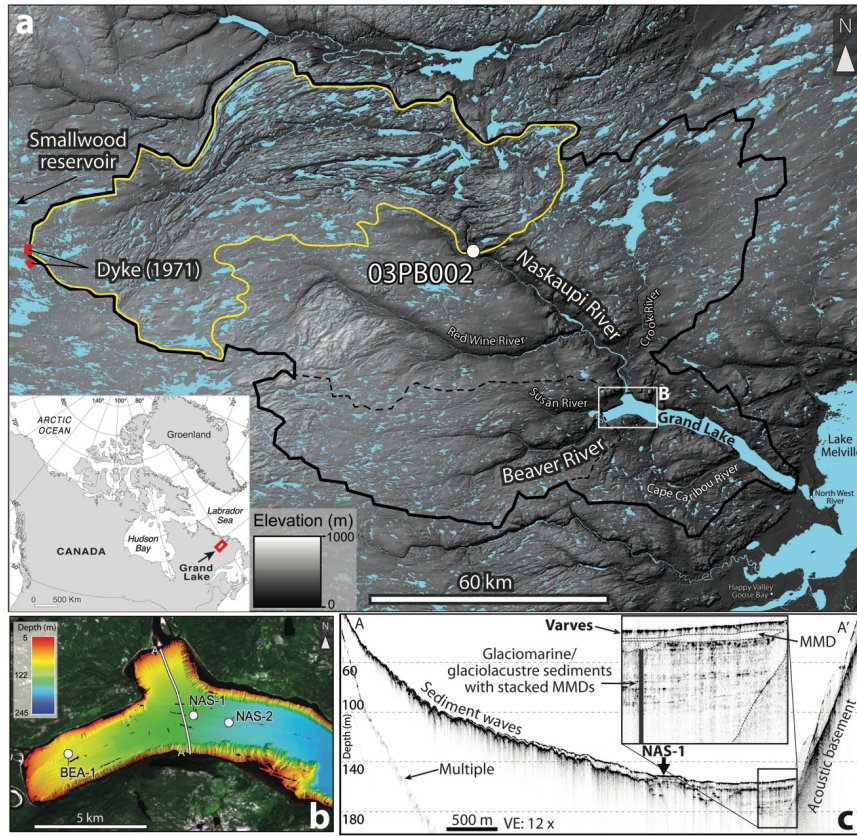
107 Grand Lake is a 245-m-deep (Trottier et al., 2020) elongated (60-km-long) fjord-lake  
108 located in a valley connected to the Lake Melville graben in central Labrador  
109 (53°41'25.58"N, 60°32'6.53"O, ~15 m above sea level) (Fig. 1). The region is part of the  
110 Grenville structural province and is dominated by Precambrian granite, gneiss and acidic  
111 intrusive rocks. Grand Lake watershed deglaciation began after ~8.2 cal ka BP (Trottier et  
112 al., 2020). During deglaciation, marine limit reached an elevation of 120-150 m above  
113 modern sea level and invaded further upstream in the modern fluvial valleys that are  
114 connected to the lake (Fizthugh, 1973). This former glaciomarine/marine sedimentary fjord

Supprimé: -climatic

116 basin has been glacio-isostatically uplifted and isolated by a morainic sill to become a deep  
117 fjord-lake (Trottier et al., 2020). The regional geomorphology is characterized by glacially  
118 sculpted bedrock exposures, glacial deposits consisting of till plateaus of various  
119 elevations, glacial lineations, drumlins, kames, eskers and raised beaches (Fulton 1992).  
120 Podzolic soils dominate, with inclusions of brunisols and wetlands.

121  
122 Grand Lake is located in the High Boreal Forest ecoregion, one of the most temperate  
123 climates in Labrador, hosting mixed forests dominated by productive, closed stands of  
124 *Abies balsamea*, *Picea mariana*, *Betula papyrifera*, and *Populus tremuloides* (Riley et al.,  
125 2013). This region is influenced by temperate continental (westerly and southwesterly  
126 winds) and maritime (Labrador Current) conditions with cool humid summers (JJA) (~8.5  
127 °C) and cold winters (DJFM) (~-13 °C). The Grand Lake watershed extends upstream over  
128 the low subarctic Nipishish-Goose ecoregion, a broad bedrock plateau (<700 m.a.s.l.)  
129 located on the west flank of the Lake Melville lowlands. Lichen-rich *Picea* woodlands with  
130 open canopies predominate. With cooler summers and longer cold winters, this area is  
131 slightly influenced by the Labrador Sea. Mean annual precipitation in the study region  
132 ranges from 800 mm to 1 000 mm, with 400 cm to 500 cm of snowfall. The regional  
133 hydrological regime typically exhibits winter low flow and spring freshet, followed by  
134 summer flow recession (Fig. 2). Snowmelt in Grand Lake region takes place from April to  
135 June (AMJ).

136



137  
 138 Figure 1. (A) Location of Grand Lake watershed (black line) and its principal tributaries. The Naskaupi  
 139 River hydrometric station (03PB002: white dot) covering an area of 4480 km<sup>2</sup> (yellow line). Location of the  
 140 dykes constructed in 1971 to divert water from the Naskaupi River to the Smallwood reservoir hydroelectric  
 141 system are also shown by the red bars. (B) High-resolution swath bathymetry (1-m resolution) of Grand Lake  
 142 (Trotter et al., 2020) coupled with a Landsat image (USGS) and core site locations. The white line indicates  
 143 the location of (C) a typical 3.5 kHz subbottom profile of the Naskaupi River delta (A-A') showing the  
 144 approximate location of core NAS-1. MMD: mass-movement deposit.

Supprimé: (C)

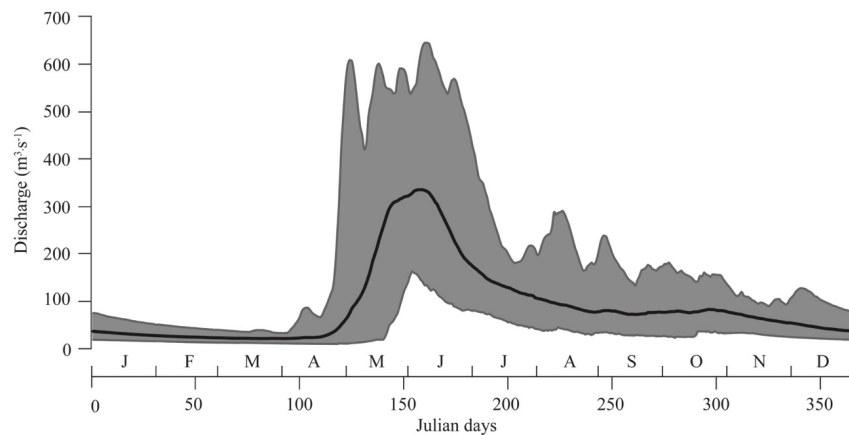
145 The main tributary of Grand Lake is the Naskaupi River located at the lake head (Fig. 1a).  
 146 The downstream part of the Naskaupi River is fed by the Red Wine and the Crook rivers.  
 147 The Beaver River is the secondary tributary of Grand Lake. Naskaupi and Beaver rivers  
 148 structural valleys that connect to the Grand Lake Basin have a well-developed fluvial plain  
 149 and a generally sinuous course that remobilize former deltaic systems and terraces  
 150 composed of glaciomarine, marine, fluvio-glacial, lacustrine and modern fluvial deposits.

152 Upstream river terraces show mass movement scarps and are affected by gully and aeolian  
153 activity. Grand Lake flows into a small tidal lake (Little Lake) and subsequently towards  
154 Lake Melville. On 28 April 1971, by closing a system of dykes, the headwaters of Naskaupi  
155 River watershed (Lake Michikamau) were diverted into the Churchill River hydropower  
156 development (Fig. 1a). This diversion has reduced the drainage area of the Naskaupi River  
157 from 23 310 km<sup>2</sup> to 12 691 km<sup>2</sup> (Anderson, 1985).

158

159 Hydroacoustic data were collected in Grand Lake in 2016 (Trottier et al., 2020). The swath  
160 bathymetric imagery and 3.5 kHz subbottom profile show that the prodelta slopes present  
161 well-defined sediment waves at the Naskaupi River mouth (Trottier et al., 2020; Fig. 1b).  
162 The upper acoustic unit is composed of a high amplitude acoustic surface changing into  
163 low amplitude acoustic parallel reflections (Fig. 1c), a type of acoustic facies which can be  
164 associated with successive sedimentary layers of contrasting particle sizes (Gilbert and  
165 Desloges, 2012).

166



167

168 *Figure 2. Observed mean daily discharges of the Naskaupi River (hydrometric station 03PB002) for the*  
169 *1978-2012 period (black line). The gray zone represents the minimum and maximum observed discharges.*

170

171 **3. Methods**

172 **3.1 Sediment coring and processing**

173 Four short sediment cores (BEA-1, NAS-1A, NAS-1B and NAS-2) were collected using a  
174 UWITEC percussion corer in March 2017 deployed from the lake ice cover. These cores  
175 were collected in undisturbed areas according to the swath bathymetry and subbottom  
176 profiling data (Trottier et al., 2020). Core BEA-1 was collected in the axis of the Beaver  
177 River at a depth of 93 m. Core NAS-1 ~~was~~ collected in the axis of the Naskaupi River at a  
178 depth of 146 ~~m~~ (Fig. 1b). Site BEA-1 and NAS-1 ~~were collected from locations sharing~~  
179 ~~relative similarities~~: at the distal frontal slope of the Beaver and Naskaupi river deltas (fig.  
180 1c). ~~Site NAS-2 was collected~~ away from the Naskaupi River delta, ~~176 m deep~~ at the  
181 beginning of the deep lake basin. ~~Sites NAS-2 is mainly fed by sediments from the~~  
182 ~~Naskaupi River, but is also in a distal position to the Beaver River~~. Duplicate cores of  
183 different lengths have been retrieved at each site to maximize undisturbed sediment  
184 recovery. Following the extraction of each core, wet floral foam was gently inserted  
185 through the top of the filled coring tube and slowly pushed towards the sediment surface  
186 to seal and preserve the sediment-water interface. A plastic cap was then installed on top  
187 of the foam to secure its position in contact with the intact sediment surface and avoid  
188 disturbance during transport of the cores. The cores were scanned using a Siemens  
189 SOMATOM Definition AS+ 128 medical CT-Scanner at the multidisciplinary laboratory  
190 of CT-scan for non-medical use of the Institut National de la Recherche Scientifique - Eau  
191 Terre Environnement (INRS-ETE). The CT-scan images allowed the identification of  
192 sedimentary structures (i.e., laminated facies, perturbation and hiatus). Expressed as CT-  
193 numbers or Hounsfield units (HU), X-Ray attenuation is a function of density and the  
194 effective atomic number, and hence sensitive to contrasts in mineralogy, grain size and  
195 sediment porosity (St-Onge et al., 2007). CT-numbers were extracted at a resolution of  
196 0.06 cm using the ImageJ software 2.0.0 (imagej.net). The cores were then opened,  
197 described and photographed with a high-resolution line-scan camera mounted on an  
198 ITRAX core scanner (RGB colour images; 50 µm-pixel size) at INRS-ETE. Geochemical  
199 non-destructive X-Ray Fluorescence (XRF) analysis was performed on the core half (30  
200 kV and 30 mA). XRF elements profiles were used to visualize the structures and boundaries

- Supprimé: and NAS-2
- Supprimé: ere
- Supprimé: and 176 m, respectively
- Supprimé: are
- Supprimé: located
- Supprimé: ; s
- Supprimé: is located

208 of the laminations and estimate particle size variability in sediment cores (Kylander et al.,  
209 2011; Cuvén et al., 2010; Croudace et al., 2006). Elements were normalized by the total of  
210 count (cps) for each spectrum. Continuous XRF measurements were also carried out on  
211 overlapping impregnated sediment blocks in order to superpose element relative intensity  
212 profiles on thin-sections.

### 213 **3.2 Chronology and thickness measurement**

214 Surface sediments from cores BEA-1 and NAS-1A were dated with  $^{137}\text{Cs}$  method (Appleby  
215 and Oldfield 1978) using a high-resolution germanium diode gamma detector and  
216 multichannel analyzer gamma counter.  $^{137}\text{Cs}$  activity was used to identify sediment  
217 deposited during 1963-1964 peak of nuclear tests and validate the annual character of the  
218 layers. A sampling interval of 2 cm was used to approximately identify the depth at which  
219 the  $^{137}\text{Cs}$  peaks were located. Subsequently, a sampling interval of  $\pm 0.5$  cm was used to  
220 sample each lamination for the period 1961-1965 to determine the exact  $^{137}\text{Cs}$  peak location  
221 (1963-1964). In order to establish a chronology for each core, detailed laminations counts  
222 were executed on CT-scan images and high-resolution photographs using ImageJ 2.0.0 and  
223 Adobe Illustrator CC softwares (Francus et al., 2002). As all of the core surface has been  
224 well preserved, the first complete lamination below the sediment surface was considered  
225 to represent the topmost year (i.e., 2016 CE). Chronology on each core was confirmed by  
226 cross-correlation between thick laminations selected as distinctive marker layers along the  
227 different sediment sequences (A to M; Fig. 4).

228

229 Thin-sections of sediments were sampled from cores BEA-1 (1856-2016), NAS-1A (1953-  
230 2016), NAS-1B (1856-1952) and NAS-2 (1968-2016) (see Fig. 4 for thin-section location)  
231 following Francus and Asikainen (2001) and Lamoureux (1994). Digital images of the thin-  
232 sections were obtained using a transparency flatbed scanner at 2400 dpi resolution (1 pixel  
233 = 10.6  $\mu\text{m}$ ) in plain light and were used to characterize lamination substructure. Lamination  
234 counts and thickness measurements using a thin-section image analysis software developed  
235 at INRS-ETE (Francus and Nobert 2007) were performed to duplicate and validate  
236 previous chronologies established on CT-Scan images and high-resolution photographs.  
237 Two counts were made from thin-section by the same observer (AGP). Total Varve

238 Thickness (TVT) and Detrital Layer Thickness (DLT) of each year of sedimentation were  
239 measured from images of thin-sections. Lamination counts made on CT-scan images, high-  
240 resolution photographs and thin-sections are identical while TVT measurements show  
241 negligible difference ( $R^2 = 0.96$ ;  $p < 0.05$ ). The thickness measurements made from CT-  
242 scan images and high-resolution photographs have been used to prolong the TVT series of  
243 core NAS-2 from 1968 back to 1856. Continuous TVT measurements allowed the  
244 establishment of high-resolution age-depth models for each site.

### 245 **3.3 Image and particle size analysis**

246 Using custom-made Image Analysis software (Francus and Nobert, 2007), regions of  
247 interest (ROIs) were selected on the thin-section images. The software then automatically  
248 yielded SEM images of the ROIs using a Zeiss Evo 50 scanning electron microscope  
249 (SEM) in backscattered electron (BSE) mode. Eight-bit greyscale BSE images with a  
250 resolution of 1024 x 768 pixels were obtained with an accelerating voltage of 20 kV, a tilt  
251 angle of 6.1 and an 8.5 mm working distance with a pixel size of 1  $\mu\text{m}$ . BSE images were  
252 processed to obtain black and white images where clastic grains ( $>3.5 \mu\text{m}$ ) and clay matrix  
253 appeared black and white respectively (Francus, 1998).

254  
255 Each sedimentary particle (an average of 2 225 particles per image) was measured  
256 according to the methodology used by Lapointe et al. (2012), Francus et al. (2002) and  
257 Francus and Karabanov (2000) in order to calculate particle size distribution on each ROI  
258 image. Due to the thickness of the laminations, results from several ROI images were  
259 merged to obtain measurements for each year of sedimentation, with an average of 4  
260 images per lamination. Only clastic facies related to spring and summer discharges were  
261 used for particle size analysis in order to exclude ice-rafted debris ( $\mu\text{m}$  to mm scale)  
262 observed in the early spring layers (see Fig. 5 for details). The 99th percentile ( $P99D_0$ ) of  
263 the particle size distribution for each detrital layer was obtained from thin-sections  
264 (Francus, 1998) for the last 160 years (1856-2016) for core BEA-1 and NAS-1, and for the  
265 last 47 years (1968-2016) for core NAS-2, from 795, 717 and 132 BSE images respectively  
266 (Fig. 4).

267

268 **3.4 Hydrological variables**

269 Hydrological variables (Tab.1) were calculated from the time series of daily discharges  
270 recorded by the Naskaupi River hydrometric station over the 1978-2011 period (missing  
271 data from the years 1996, 1997 and 1998).

272

273 *Table 1. Hydrological variables used in this paper*

Hydrological variable	Unit	Description
Q-max	m <sup>3</sup> /s	Annual maximum of daily discharges
Q-mean	m <sup>3</sup> /s	Mean annual discharge
Q-max-Jd	Julian days	Julian day at which the discharge reaches its maximum annual value
Rise-Time	Days	Number of days between the minimum winter flow and the maximum spring flow
Nb-Days-SupQ80	Days	Number of days with discharge greater than the 80 <sup>th</sup> daily percentile
Q-nival	mm	Nival runoff (April, May, June, July)

274

275

276 The Naskaupi River hydrological variables have been compared with four other  
277 hydrometric station data available around the study region (Fig. 3a, Tab. 2), which are  
278 devoid of anthropogenic perturbations. Q-mean series from the five stations have been  
279 normalized for the common 1979–2011 period and averaged, to produce a Labrador region  
280 mean annual discharge series. This allows to extend instrumental data series for the period  
281 1969 to 2011, and fill in data for the missing years. The Labrador hydrometric station data  
282 used in this study come from a Government of Canada website (<https://wateroffice.ec.gc.ca>  
283 05/2018).

284

285 *Table 2. Description of hydrometric stations used in this study*

Hydrometric station	ID	Area (km <sup>2</sup> )	Location (N,W)	Recording period
Ugjoctok River	03NF001	7570	55° 14' 02", 61° 18' 06"	1979-2011
Naskaupi River	03PB002	4480	54° 07' 54", 61° 25' 36"	1978-2011
Minipi River	03OE003	2330	52° 36' 45", 61° 11' 07"	1979-2011
Little Mecatina River	02XA003	4540	52° 13' 47", 61° 19' 01"	1979-2011
Eagle River	03QC001	10 900	53° 32' 03", 57° 29' 37"	1969-2011

286

287

Supprimé: -climatic

Supprimé: -climatic

290 **3.5 Varve physical parameters and hydrological variables**

291 A simple linear regression model was used to fit the DLT and P99D<sub>0</sub> series with local  
292 (1978-2011) and regional (1969–2011) instrumental series and reconstructed hydrological  
293 variables (Q-mean, Q-max) back to 1856. Model calibration was performed using a  
294 twofold cross-validation technique over the instrumental period. Root mean squared errors  
295 (RMSE) and coefficient of determination ( $R^2$ ) were calculated for calibration periods,  
296 while average reduction of error (RE) and average coefficient of efficiency (CE) were  
297 calculated to evaluate reconstruction skills (Briffa et al. 1988, Cook et al., 1999). The RE  
298 and CE of the verification periods must be  $> 0$  to validate the model skills. Statistical  
299 analysis was realized using the treeclim package (Zang and Biondi, 2015) in the R-project  
300 environment (R Core Team, 2019, <http://www.r-project.org/>).

301

302 **3.6 Hydro-climatic reconstruction based on rainfall-runoff modelling**

303 The applied reconstruction method is based on rainfall-runoff modelling. Firstly, it aims at  
304 producing, for the Naskaupi River hydrometric station catchment (Fig. 1a), daily climatic  
305 time series using a historical reanalysis of global geopotential height fields extracted over  
306 the studied region for a given time period (here 1880-2011). Secondly, the produced  
307 climatic series are used as inputs to a rainfall–runoff model previously calibrated on the  
308 studied catchment in order to obtain daily streamflow time series. The reconstruction  
309 method is fully described in Brigode et al. (2016) and was recently applied over  
310 southeastern Canada catchments in Dinis et al. (2019). It is summarized in the following  
311 paragraphs.

312

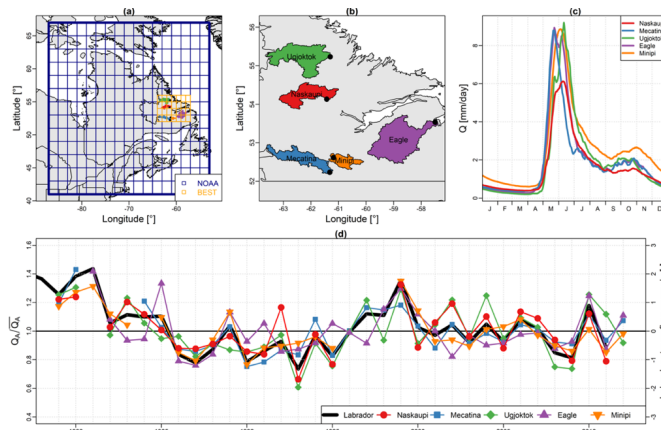
313 The available observed hydro-climatic series for the Naskaupi River hydrometric station  
314 catchment have been aggregated at the catchment scale. Climatic series (daily air  
315 temperature and precipitation) have been extracted from the CANOPEX dataset (Arsenault  
316 et al., 2016), built using Environment Canada weather stations and Thiessen polygons to  
317 calculate climatic series at the catchment scale. Daily air temperature series have been used  
318 for calculating daily potential evapotranspiration at the catchment scale, using the Oudin  
319 et al. (2005) formula designed for rainfall-runoff modelling.

320

321 These daily series have been used for calibrating the GR4J rainfall-runoff model (Perrin et  
 322 al., 2003) and its snow accumulation and melting module, CemaNeige (Valéry et al.,  
 323 2014a), using the airGR package (Coron et al., 2017). This combination of GR4J and  
 324 CemaNeige (hereafter denoted CemaNeigeGR4J) has been recently applied over eastern  
 325 Canada catchments and showed good modelling performances (e.g., Seiller et al., 2012;  
 326 Valéry et al., 2014b, Brigode et al., 2016). CemaNeigeGR4J has been calibrated on the  
 327 recorded period of the Naskaupi River hydrometric station catchment using the Kling and  
 328 Gupta efficiency criterion (Gupta et al., 2009) as objective function.

329  
 330 Then, the observed climatic series have been resampled over the 1880-2011 period, based  
 331 on both season and similarity of geopotential height fields (Kuentz et al., 2015). The  
 332 resampling is performed by calculating Teweles and Wobus (1954) distances between four  
 333 geopotential height fields: (i) 1000 hPa at 0 h, (ii) 1000 hPa at 24 h, (iii) 500 hPa at 0 h,  
 334 and (iv) 500 hPa at 24 h. The NOAA 20<sup>th</sup> Century Reanalysis ensemble (Compo et al.,  
 335 2011, hereafter denoted 20CR) has been used as a source of geopotential height fields (Fig.  
 336 3b).

337



338  
 339 *Figure 3. (a) Dataset used for the hydro-climatic reconstruction based on rainfall-runoff modelling: the*  
 340 *extension of the 20CR grid used is shown in blue, while the BEST grid used is highlighted in orange. (b)*  
 341 *Spatial distribution of hydrometric stations used in this study (black dots) and their catchment area. (c)*  
 342 *Observed mean daily discharges of each hydrometric station for the 1978-2012 period. (d) Labrador*  
 343 *streamflow anomaly and the Labrador region mean annual discharge series (thick black line).*

344 As in Brigode et al. (2016), the resampled series of air temperature have been corrected at  
345 the catchment scale using a regression model calibrated with the Berkeley Earth Surface  
346 Temperature analysis (Rohde et al., 2013, hereafter denoted BEST). BEST is a gridded air  
347 temperature product starting in 1880 at the daily timestep (Fig. 3b).

348

349 Finally, the daily climatic series are used as inputs to the CemaNeigeGR4J model in order  
350 to obtain daily streamflow time series on the same 1880-2011 period. Thus, the outputs of  
351 the hydro-climatic reconstruction are an ensemble of daily meteorological series (air  
352 temperature, potential evapotranspiration and precipitation) and an ensemble of daily  
353 streamflow series.

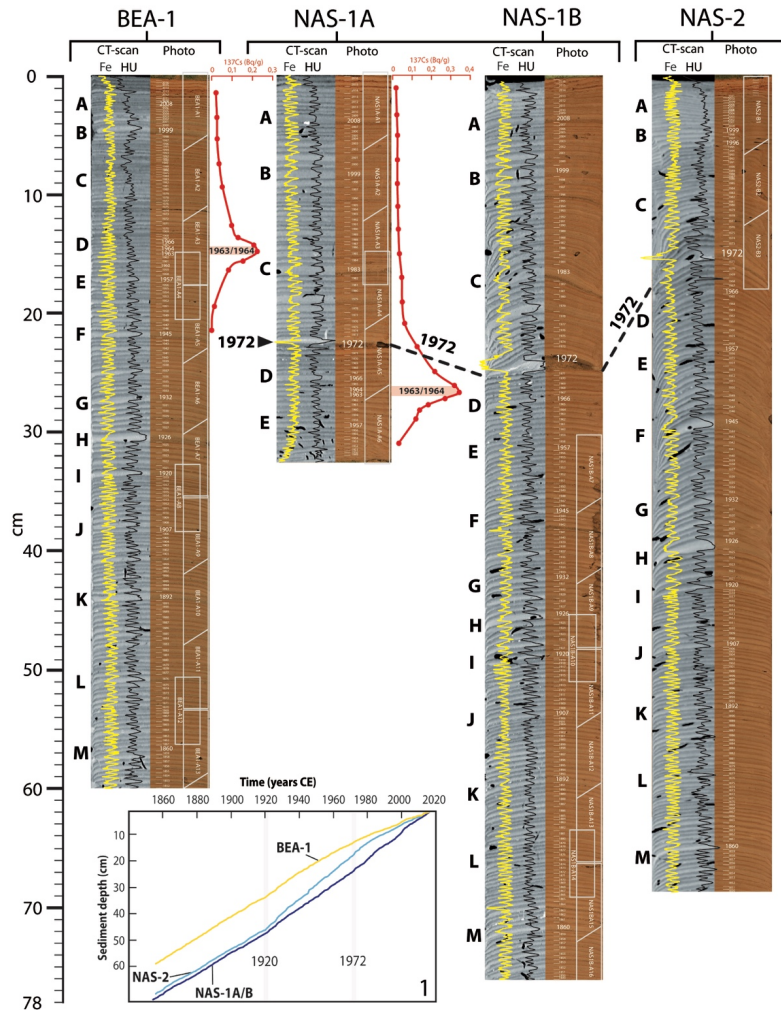
354

## 355 **4. Results**

### 356 **4.1 Lamination characterization**

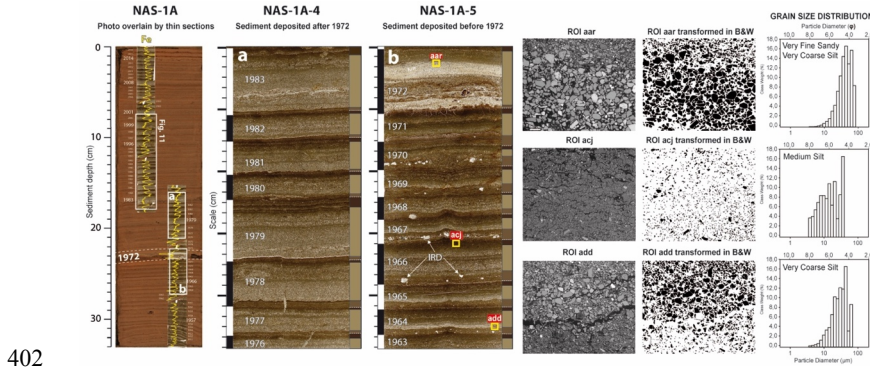
357 Sediment retrieved at the head of Grand Lake (Fig. 4), consist of dark grayish to dark  
358 yellowish brown (Munsell colour: 10YR-4/2 to 10YR-4/4) laminated minerogenic  
359 material, interpreted as clastic lamination of fluvial origin. Lamination structure can be  
360 divided in 3 seasonal layers (Fig. 5) based on their stratigraphic position and microfacies.  
361 Annual sedimentation starts with a layer composed of silt and clay sediment matrix which  
362 sometimes contains ice-rafted debris ( $\mu\text{m}$  to  $\text{mm}$  scale) interpreted as an early spring layer.  
363 The major lamination component is a spring and summer/autumn detrital layer. Its thick  
364 basal part is mostly poorly sorted, graded and composed of coarse minerogenic grains  
365 comprising fine sand and silts ( $< 150 \mu\text{m}$ ) with some redeposited cohesive sediment clasts  
366 eroded from the underlying early spring layer. This detrital layer has a sharp lower  
367 boundary. The upper part of the detrital layer consists of a finer detrital grain matrix  
368 containing thin visually coarser intercalated sub-layers in  $\sim 75\%$  of the laminations. The  
369 allochthonous lithoclastic materials which compose the detrital layers are associated with  
370 higher density values (Fig. 4) and an increase in the relative intensity of elements Sr and  
371 Ca (Zolitschka et al., 2015). Few organic debris and charcoal fragments are observed  
372 throughout the detrital layers. The third topmost lamination layer is formed by a fine to  
373 medium silty layer with abundant clay rich in Fe and interpreted as an autumn and winter  
374 layer, also known as a clay cap (Zolitschka et al., 2015). The Fe peak values in autumn and

375 winter layers, are hence used to determine the upper lamination boundary (Fig. 4)  
 376 (Zolitschka et al., 2015) as previously performed in other varved sequences (Cuven et al.,  
 377 2010; Saarni et al., 2016).



378  
 379 Figure 4. Varve counts made on (left) CT-scan and (right) high resolution images from core BEA-1, NAS-  
 380 1A/B and NAS-2. Distinctive marker layers are identified by letters A to M. The 1972 marker layer is outlined  
 381 by the thick dark gray line. Fe relative intensity and density (HU) profile represented by the yellow and black  
 382 line respectively, show rhythmic laminations. The activity profile of  $^{137}\text{Cs}$  in core BEA-1, NAS-1A is shown  
 383 by the red line. Approximate thin-section locations are outlined by white boxes. The age-depth model of the  
 384 3 cores is also presented (Box. 1). See Fig. 1b for core locations.

385 The lamination deposited in 1972 from sites in the axis of the Naskaupi River (NAS-1; Fig.  
 386 5b and NAS-2; Fig. 4), present a thick (8.2 mm) and coarse (67.8  $\mu\text{m}$ ) detrital layer  
 387 composed of very fine sandy and very coarse silt (Fig. 5b) representing the highest particle  
 388 size measured in all sequences. Furthermore, there is a difference in lamination physical  
 389 parameters and microfacies deposited before and after the 1972 marker bed, especially in  
 390 core NAS-1, the proximal site from the Naskaupi River mouth. Laminations deposited  
 391 prior 1972 have a well-developed substructure relatively constant among each annual  
 392 lamination (Fig. 5b). The early spring layer of the pre-1972 laminations is thicker and more  
 393 clearly visible. Conversely, the detrital layer of laminations post-1972 is thicker, while the  
 394 early spring layer is more difficult to discern and contributes less to the TVT (Fig. 5a). The  
 395 mean contribution of the early spring layer and autumn and winter layer to the total  
 396 lamination thickness is 35% for the pre- and 52% for the post-1972 intervals. The early  
 397 spring layer in lamination post-1971 from sites NAS-1 and NAS-2 no longer contains  
 398 isolated coarse debris. The changes in lamination facies are less noticeable in core NAS-2,  
 399 which was sampled further away from the Naskaupi River mouth. The 1972 marker bed  
 400 and related facies changes are not found at the Beaver River mouth site BEA-1.  
 401



402  
 403 *Figure 5. (Left) Photo of core NAS-1A overlain by thin-section image and Fe relative intensity profile (yellow*  
 404 *lines). The 1972 marker layer is outlined by the white dashed lines. Thin-section images showing sedimentary*  
 405 *structure of varves deposited (B) before and (A) after the 1972 marker bed. Varve boundaries are represented*  
 406 *by the vertical black and white bars. Varve layers are delimited by the medium brown (early spring layer),*  
 407 *pale brown (detrital layer) and dark brown (autumn and winter layer) bars. Typical Ice-Rafted Debris (IRD)*  
 408 *are shown by the white arrows on the b panel. (Right) BSE images of three ROIs transformed in B&W and*  
 409 *their associated particle size distribution (aar: the 1972 marker layer; acj: a typical autumn and winter*  
 410 *layer; add: the base of a typical detrital layer) (see yellow squares on the b panel for ROIs location).*

411 **4.2 Varve chronology**

412 The laminated sequences chronologies are consistent with the Cesium-137 main peaks  
413 corresponding to the highest atmospheric nuclear testing period (1963-1964 CE) (Appleby,  
414 2001). Peaks are found at 14-14.5 cm (BEA-1) and 26.5-27 cm (NAS-1A) depth (Fig. 4)  
415 and perfectly match the lamination counts in both cores, confirming the varve assumption.  
416 The presence of the distinct 1972 marker layer at this chronostratigraphic position in the  
417 varve sequence which coincides with the occurrence of the Naskaupi River diversion that  
418 took place in April 1971 (see section 5.2 for details) supports the reliability of the  
419 constructed chronologies.

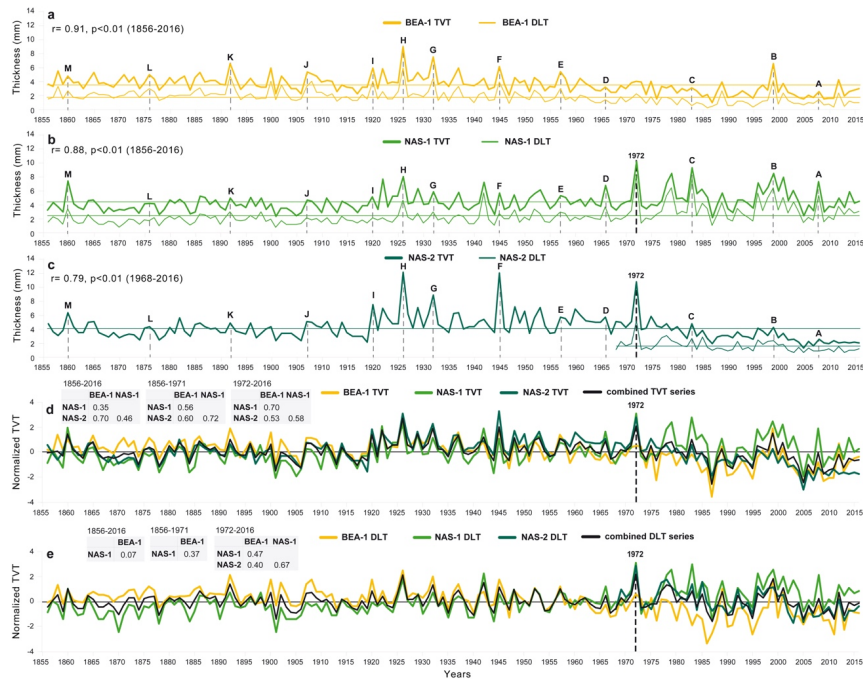
420

421 Independent varve chronologies were established from sediment cores BEA-1, NAS-1 and  
422 NAS-2 (Fig. 4). A total of 160 varves were counted at each site, covering the 1856-2016  
423 period. The thickness and the good quality of the well-preserved varve structures allowed  
424 a robust age-model reproducible among cores to be constructed. Despite the distance  
425 between the coring sites (1 to 5 km) and the two different sediment sources (Naskaupi and  
426 Beaver River) (Fig. 1b), there is no varve count difference between the selected thick  
427 marker layers (A to M; Fig. 4) among cores. The few counting difficulties occur within  
428 varve years 1952-1953, 1935-1934, 1918-1919, as it contains ambiguous coarse non-  
429 annual intercalated sub-layers with intermediate clay cap that can be interpreted as one year  
430 of sedimentation. Both varve counts performed on thin-sections show a low overall  
431 counting error ( $\pm 1.8\%$ ) which demonstrated the precision and accuracy of the varve  
432 sequences chronology. The age-depth models (Fig. 4, Box. 1) show changes in sediment  
433 accumulation rates (thickness) among cores in 1920 and 1972.

434 **4.3 Thickness and particle size measurements**

435 The TVTs from core BEA-1, NAS-1 and NAS-2 vary between 0.9 and 12.9 mm, with an  
436 average thickness of 4.09 mm (Fig. 6a, b, c, Supplements Fig. S1 and Tab. S1). The DLTs  
437 vary between 0.3 and 8.3 mm, with an average thickness of 1.9 mm (Fig. 6a, b, c,  
438 Supplements Fig. S2 and Tab. S2). There are significant strong positive correlations  
439 between TVT and DLT for each core ( $r = 0.79$  to  $0.91$ ;  $p < 0.01$ ). A step in the TVT is  
440 observable in the early 1920s at the three sites (Fig. 6a, b, c), especially in core NAS-2,

441 which recorded their highest values (12.9 mm) during the 1920-1972 period (Fig. 6c).  
442 Since the 1920s, there is a statistically significant decreasing trend in TVTs and DLTs in  
443 core BEA-1 (Fig. 6a). Thickness data from the three sites have been normalized and  
444 averaged to produce combined TVT and DLT series (Fig. 6d, e). From 1920 to 1972,  
445 combined TVT and DLT series show a statistically significant downward trend, despite an  
446 increase in years associated with high thickness values. Overall, TVT and DLT vary  
447 similarly in time between sites during the 1856-1971 period (Fig. 6d, e). However, after  
448 1972, TVT and DLT series are more diverging. From 1972 to 2016, there is a statistically  
449 significant decreasing trend in TVT and DLT in cores NAS-2 (Fig. 6c), and the amplitude  
450 of their variability tends to diminish. For core NAS-1 (Fig. 6b), post-1971 period is  
451 associated with higher thickness values. Core NAS-1 has recorded a slight TVT and DLT  
452 decrease for the 1972-2016 period, but unlike the other cores, the variability tends to  
453 increase. The TVT and DLT are overall finer in the distal core NAS-2 compared to the  
454 more proximal core NAS-1 (Fig. 4, Box. 1, Supplements Tab. S1, S2).  
455

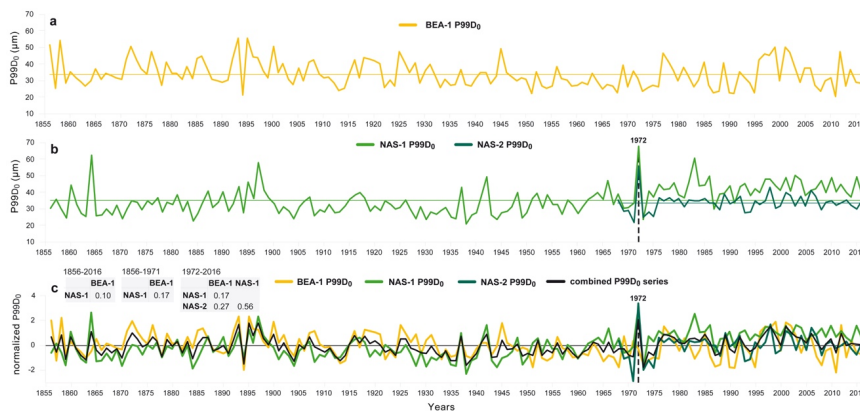


456  
 457 *Figure 6. Total Varve Thickness (TVT; thick line) and Detrital Layer Thickness (DLT; thin line) time series*  
 458 *of core (a) BEA-1, (b) NAS-1 and (c) NAS-2. Normalized (d) TVT and (e) DLT series and the combined series*  
 459 *(mean of the normalized data from the 3 sites). Pearson correlation coefficients between TVT and DLT for*  
 460 *the 1856-2016, 1856-1971 and 1973-2016 periods are shown. The selected marker layers are identified by*  
 461 *letters A to M and the 1972 marker layer is outlined by the thick black dashed line.*

462 The P99D<sub>0</sub> of cores BEA-1, NAS-1 and NAS-2 vary between 20 and 67.8 μm, with an  
 463 average value of 34.3 μm (Fig. 7, Supplements Fig. S3 and Tab. S3). The grain size is finer  
 464 in core NAS-2 compared to core NAS-1. Particle size data from the three sites have been  
 465 normalized and averaged to produce combined P99D<sub>0</sub> series (Fig. 7c). The combined  
 466 P99D<sub>0</sub> series show a slight coarsening trend towards the end of the 19<sup>th</sup> century. From 1900  
 467 to 1971, P99D<sub>0</sub> values are generally below average. The 1972 marker layer of core NAS-  
 468 1 presented the maximum P99D<sub>0</sub> values (Fig. 7b). After 1972, there is an increase of P99D<sub>0</sub>  
 469 values in core NAS-1, where a step is observable. Pre-1971 varves in core NAS-1 have a  
 470 mean P99D<sub>0</sub> of 32,47 μm compared to 42,91 μm for the 1972-2016 period.

471

472 There is weak to moderate positive correlation between TVT and P99D<sub>0</sub> from a same core  
 473 (BEA-1:  $r = 0.41$   $p < 0.01$ ; NAS-1:  $r = 0.52$   $p < 0.01$ ; NAS-2:  $r = 0.27$ ,  $p < 0.05$ ). The  
 474 correlation between DLT with P99D<sub>0</sub> is stronger (BEA-1:  $r = 0.49$   $p < 0.01$ ; NAS-1:  $r =$   
 475  $0.65$   $p < 0.01$ ; NAS-2:  $r = 0.49$ ,  $p < 0.01$ ). Thick varves are more likely to have high grain  
 476 size values. However, these correlations show that TVT, DLT and P99D<sub>0</sub> remain  
 477 independent variables and can both reveal different hydrological information.  
 478



479  
 480 *Figure 7. P99D<sub>0</sub> time series of cores (a) BEA-1, (b) NAS-1 (1856-2016) and NAS-2 (1968-2016). (c)*  
 481 *Normalized P99D<sub>0</sub> series and the combined series (mean of the normalized data from the 3 sites). The 1972*  
 482 *marker layer is outlined by the black dashed line. Pearson correlation coefficients between P99D<sub>0</sub> series for*  
 483 *the 1856-2016 and 1968-2016 periods are shown.*

#### 484 4.5 Relation between varve series and instrumental record

##### 485 4.5.1 Naskaupi River

486 To examine how the physical parameters of the varves are related to local hydrology and  
 487 to demonstrate their potential for hydrological reconstruction, sediment parameters (TVT,  
 488 DLT and P99D<sub>0</sub>) of each core were systematically compared to hydrological variables  
 489 (Tab. 1). TVT, DLT and P99D<sub>0</sub> series from the three coring sites show significant positive  
 490 correlations with the Q-mean and Q-max extracted from the Naskaupi River hydrometric  
 491 station (03PB002) data on the 1978-2011 period ( $n=31$ ) (Tab. 3). The TVT and DLT of  
 492 cores BEA-1 and NAS-2 show stronger correlation with Q-mean, while TVT and DLT of  
 493 cores NAS-1 have a better relation with Q-max. There is a significant negative correlation  
 494 between P99D<sub>0</sub> of core NAS-1 and Q-max-Jd ( $r = -0.38$ ) and Rise-Time ( $r = -0.47$ ).  
 495 Sediment parameters also present significant positive correlations with Q-Nival ( $r = 0.32$

Supprimé: hydroclimate

497 to 0.61) and Nb-days-SupQ80 ( $> 125 \text{ m}^3 \cdot \text{s}^{-1}$ ) ( $r = 0.44$  to  $0.62$ ). Combined DLT and P99D<sub>0</sub>  
498 series (Fig. 6d, e; 7c) yields the strongest correlations in our dataset ( $r = 0.68$  and  $0.75$ ;  
499 Tab. 3) and have been used to reconstruct Naskaupi River Q-mean and Q-max respectively  
500 (Fig. 8).

501

#### 502 4.5.2 Labrador region

503 To determine if there is a regional hydrological signal in Labrador and whether the Grand  
504 Lake varved sedimentary sequence has recorded this signal, the Naskaupi River  
505 hydrological variables were compared with other Labrador hydrometric stations (Tab. 2).

506 Despite specific local geomorphological and climatic conditions, strong similarities exist  
507 between observed mean daily discharges (Fig. 3c) and annual streamflow (Fig. 3d)  
508 recorded by hydrometric stations in Labrador for the 1978-2011 period. The shape of the  
509 five annual regimes shows similar characteristics (i.e. flood-timing, strength, duration,  
510 snowmelt and rainfall response). The instrumental Naskaupi River mean annual discharge  
511 series data show significant ( $p < 0.01$ , Supplements Tab. S5) positive correlations with  
512 other hydrometric stations (Ugjoctok:  $r = 0.84$ ; Minipi:  $r = 0.70$ ; Little Mecatina:  $r = 0.73$ ;  
513 Eagle:  $r = 0.49$ ). Hydrological conditions in the Naskaupi river region is thus representative  
514 of a broader region of Labrador. Therefore, the combined DLT series (without the NAS-1  
515 1978-2016 period) has been used to reconstruct the Labrador region mean annual discharge  
516 series (Fig. 9).

517

Supprimé: Snow-Win ( $r = 0.47$  to  $0.61$ )

Supprimé: Moreover, the maximum particle size series of core NAS-1 show significant ( $p = 0.02$ ) positive correlations with the average spring temperature ( $r = 0.40$ ; not shown in Tab. 3).

Supprimé: -climatic

524 Table 3. Matrix of correlation coefficients (Pearson *r*) of the hydrological variables defined in Tab.  
 525 1 with Total Varve Thickness (TVT), Detrital Layer Thickness (DLT) and particle size (P99D<sub>0</sub>) on  
 526 the instrumental period (1978-2011; n=31) for each core. Correlations between the hydrological  
 527 variables and the combined TVT, DLT and P99D<sub>0</sub> series (normalized and averaged varve  
 528 parameters of cores BEA, NAS-1 and NAS-2) are also present. Correlations in boldface are  
 529 significant at *p* < 0.05 (Supplements Tab. S4). Correlations marked by an asterisk were used for the  
 530 final Q-mean and Q-max reconstructions.

Supprimé: -climatic

Supprimé: -climatic

		Hydrological variables of station 03PB002					
Sediment parameters	<b>Core BEA-1</b>	Q-mean	Q-max	Q-max-Jd	Rise-Time	Nb-days-supQ80	Q-nival
	TVT	<b>0,53</b>	<b>0,46</b>	-0.19	-0.06	<b>0,54</b>	<b>0,41</b>
	DLT	<b>0,54</b>	<b>0,38</b>	-0.01	0.22	<b>0,44</b>	<b>0,32</b>
	P99D <sub>0</sub>	<b>0,56</b>	<b>0,56</b>	-0.05	0.17	0.34	<b>0,40</b>
	<b>Core NAS-1</b>	Q-mean	Q-max	Q-max-Jd	Rise-Time	Nb-days-supQ80	Q-nival
	TVT	<b>0,52</b>	<b>0,64</b>	-0,31	-0,26	<b>0,55</b>	<b>0,56</b>
	DLT	<b>0,53</b>	<b>0,67</b>	-0,31	-0,27	<b>0,53</b>	<b>0,54</b>
	P99D <sub>0</sub>	0.19	<b>0,60</b>	<b>-0,38</b>	<b>-0,47</b>	0,26	<b>0,40</b>
	<b>Core NAS-2</b>	Q-mean	Q-max	Q-max-Jd	Rise-Time	Nb-days-supQ80	Q-nival
	TVT	<b>0,49</b>	<b>0,45</b>	0,04	-0,24	<b>0,56</b>	<b>0,47</b>
	DLT	<b>0,62</b>	<b>0,57</b>	0,07	-0,13	<b>0,59</b>	<b>0,61</b>
	P99D <sub>0</sub>	0,39	<b>0,43</b>	0,19	0,26	0,31	<b>0,40</b>
	<b>Mean series</b>	Q-mean	Q-max	Q-max-Jd	Rise-Time	Nb-days-supQ80	Q-nival
	TVT	<b>0,56</b>	<b>0,58</b>	-0,19	-0,20	<b>0,60</b>	<b>0,53</b>
	DLT	<b>0,68*</b>	<b>0,65</b>	-0,11	-0,07	<b>0,62</b>	<b>0,58</b>
P99D <sub>0</sub>	<b>0,59</b>	<b>0,75*</b>	-0,09	0,05	<b>0,43</b>	<b>0,56</b>	

531

## 532 4.6 Hydrological reconstructions using varve parameters

### 533 4.6.1 Naskaupi River Q-mean and Q-max

534 The Naskaupi River mean and maximum annual discharges (Q-mean and Q-max) were  
 535 reconstructed using DLT and P99D<sub>0</sub> series for the 1856–2016 period. The reconstructions  
 536 were performed using single-core data, combined DLT and P99D<sub>0</sub> series and other  
 537 combinations of core data, in order to propose the most relevant reconstructions  
 538 (Supplements Fig. S4, S5). The observations and the reconstructed Q-mean and Q-max  
 539 extracted from the different series over the 1978-2011 period are consistent. Despite  
 540 differences, all reconstructions tested using different sources of sedimentological data  
 541 generally share common interannual and longer-term variability.

542

545 Excluding the 1972-2016 measurements from NAS-1 from the combined series for  
546 reconstructions was also tested to remove the likely anthropogenic impact on sedimentation  
547 during this period. The combined DLT series without the 1972-2016 period presents a  
548 slightly better fit with the instrumental data (lowest RMSE and the most-significant and  
549 highest  $R^2$ , Supplements Tab. S6). The model calibrations based on a twofold cross-  
550 validation reveal that this DLT series has better overall predictive capacity to reconstructed  
551 Q-mean (Supplements Tab. S7). The 1972-2016 period of core NAS-1 was then excluded  
552 from the combined DLT series used to perform the best reconstruction of Naskaupi River  
553 Q-mean presented in Fig. 8a. However, significantly stronger calibration and validation  
554 statistical results were obtained by keeping this period in the combined P99D<sub>0</sub> series used  
555 to reconstruct Naskaupi River Q-max (Fig. 8b, Supplements Tab. S8, S9). The varve of  
556 year 1972 is considered as an outlier that originated from anthropogenic impacts, and thus  
557 was not included in all reconstructions.

558

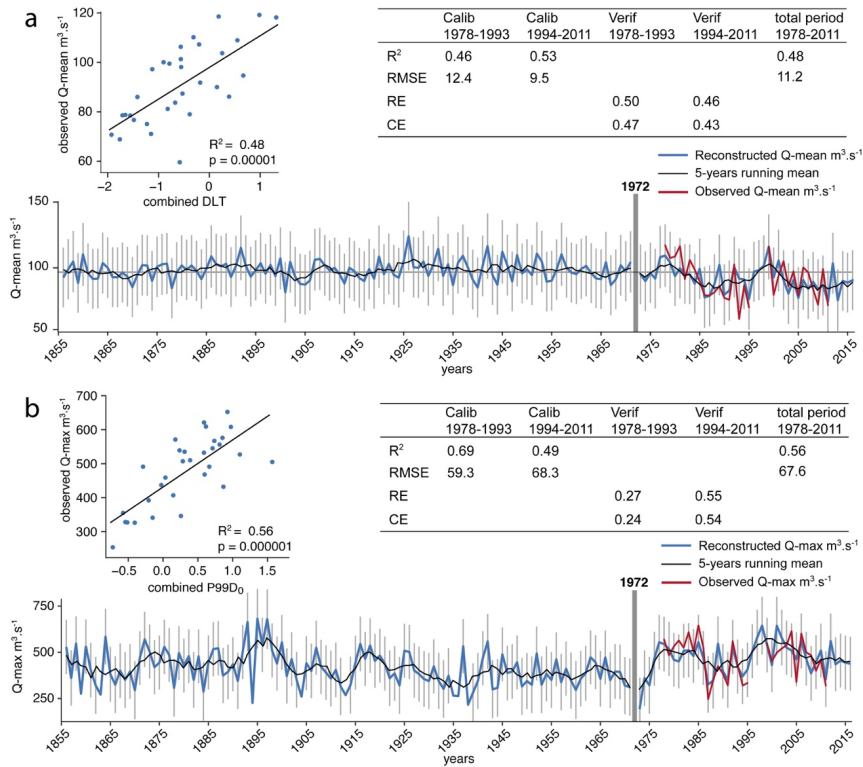
559 The reconstructed Naskaupi River Q-mean from combined DLT series varies between 73  
560 and 126  $\text{m}^3\cdot\text{s}^{-1}$ , with an average of 96  $\text{m}^3\cdot\text{s}^{-1}$  (Fig. 8a), and remains relatively stable from  
561 1856 to 1920, mainly near average. Several years with high Q-mean occurred during the  
562 1920-1960 period. A statistically significant downward trend of the Q-mean is observed  
563 over the last 90 years. Recently, high Q-mean periods are observed from 1976 to 1985 and  
564 1996 to 2002 and lower Q-mean periods from 1986 to 1995 and 2003 to 2016. The  
565 reconstructed Naskaupi Q-max from combined P99D<sub>0</sub> series varies between 192 and 681  
566  $\text{m}^3\cdot\text{s}^{-1}$ , with an average of 426  $\text{m}^3\cdot\text{s}^{-1}$  (Fig. 8b). There is a slight upward trend in Q-max at  
567 the end of the 19th century. The 1900-1971 period is characterized by a Q-max generally  
568 below average. Three periods of high Q-max are observed from 1887 to 1900, 1976 to  
569 1986 and 1995 to 2008 (Fig. 8b).

570

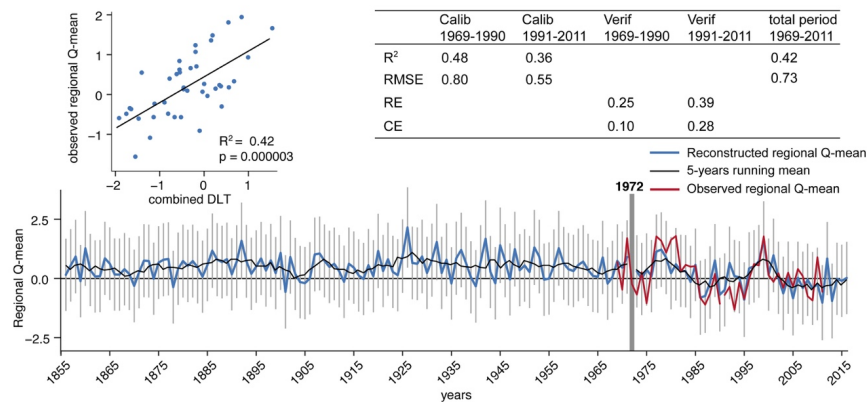
#### 571 *4.6.2 Labrador region Q-mean*

572 The consistency between combined DLT series and the observed Labrador region Q-mean  
573 series (Fig. 9), based on the discharge variability of five watersheds of different size and  
574 location, demonstrates that the Grand Lake varved sequence contains a regional signal. The  
575 best reconstruction of Labrador region mean annual discharges is the one performed using

576 the combined DLT series without the NAS-1 1972-2016 period. This reconstruction  
 577 demonstrates the best predictive capacity (RE and CE must be > 0 to validate the model  
 578 skills, Supplements Tab. S10, S11). The regional Q-mean reconstruction for the 1856-  
 579 2016 period is presented in Fig. 9.  
 580



581  
 582 *Figure 8. Naskaupi River (a) Q-mean and (b) Q-max reconstructed from combined DLT (Without the NAS-*  
 583 *1 1978-2016 period) and P99D<sub>0</sub> series respectively, for the 1856-2016 period (blue line), with 5-year*  
 584 *moving average (black line). Error bars represent the 95% confidence interval. Observed Q-mean and Q-*  
 585 *max are also shown for the 1978-2011 period (red line).*



586  
587  
588  
589  
590

Figure 9. Labrador region Q-mean reconstructed from combined DLT series (without the NAS-1 1972-2016 period) for the 1856–2016 period (blue line), with 5-year moving average (black line). Error bars represent the 95% confidence interval. Observed Labrador region Q-mean series is also shown for the 1969-2011 period (red line).

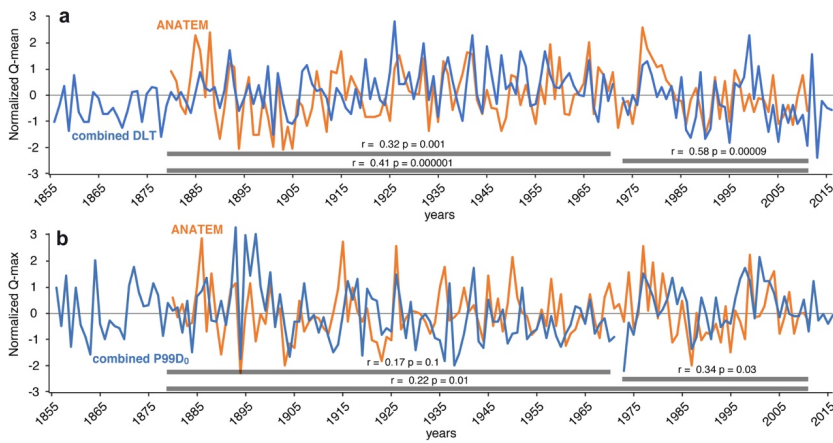
591 **4.7 Hydrological reconstruction using the rainfall-runoff modelling approach and**  
592 **comparison with the varved-based reconstruction**

593 Naskaupi River Q-mean and Q-max (Fig. 8) were also reconstructed using the ANATEM  
594 rainfall-runoff modelling (Fig. 10). The independent modelling approach results show  
595 similarities with reconstructions based on varved series. The ANATEM reconstructions are  
596 statistically and positively correlated with the yearly time series obtained from combined  
597 DLT and P99D<sub>0</sub> series during the 1880-2011 period (Q-mean:  $r = 0.41$ ; Q-max:  $r = 0.22$ ;  $n = 131$ ;  
598  $p < 0.01$ ). The reconstructed Q-mean and Q-max annual variabilities show  
599 similarities, especially during the 1973–2011 period (Q-mean:  $r = 0.58$ ; Q-max:  $r = 0.34$ ;  
600  $n = 43$   $p < 0.05$ ).

601

602 Q-mean reconstructions with both varve parameters and modelling are better correlated  
603 than the Q-max reconstructions. This may be due to the higher uncertainty related to the  
604 Q-max reconstruction with the modelling approach. Indeed, high flow modelling requires  
605 good reconstruction performances on several hydro-climatic processes (i.e., snow  
606 accumulation during the winter, timing of the snowmelt, spring precipitation). Moreover,  
607 the uncertainty of the hydrological reconstruction is less important on recent periods  
608 (>1950), due to the better quality of the geopotential height field reanalysis over recent  
609 decades, as more stations series are available and thus used in the reanalysis. The decrease

610 in the uncertainty related to reanalysis over time might explain the better correlation  
 611 between the two approaches for the recent period.



612  
 613 *Figure 10. Comparison between the Naskaupi River (a) Q-mean and (b) Q-max reconstruction using*  
 614 *combined Detrital Layer Thickness (DLT) (without the NAS-1 1972-2016 period) and P99D<sub>0</sub> series*  
 615 *respectively (blue line) and the rainfall-runoff modelling (orange line) for raw yearly data.*

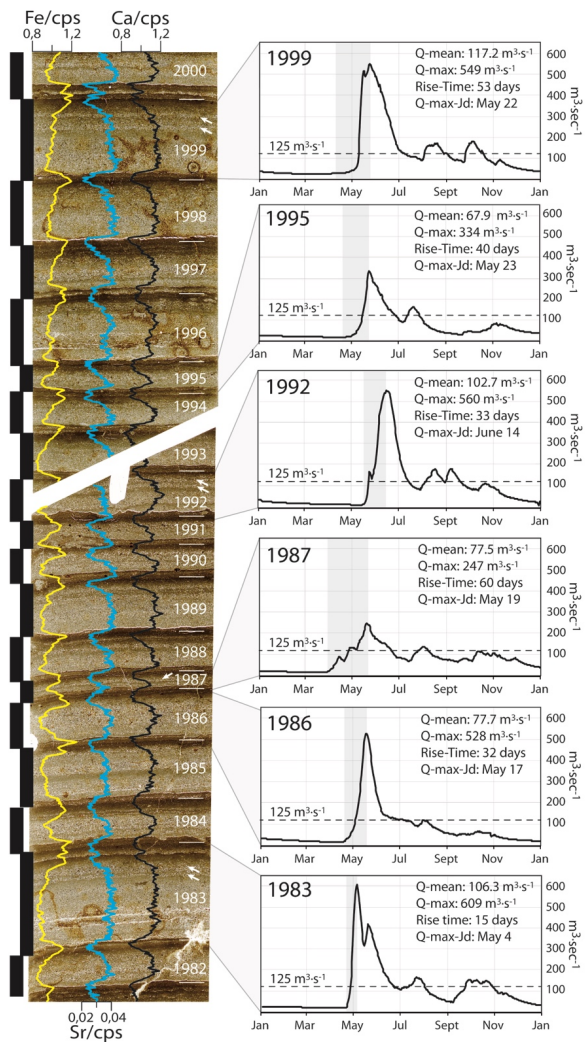
616 **5. Discussion**

617 **5.1 Grand Lake varve formation**

618 Lakes containing well-defined and continuous varved sequences that allow the  
619 establishment of an internal chronology are rare in boreal regions. However, the great depth  
620 of Grand Lake, the availability of fine sediments in its watershed due to the glacial and  
621 postglacial history of the region (Trottier et al., 2020), as well as its important seasonal  
622 river inflow have favoured the formation and preservation of exquisite and thick varves.  
623 The seasonal streamflow regime plays a significant role in the annual cycle of  
624 sedimentation in Grand Lake and is responsible for the formation of the three distinct varve  
625 layers. Due to the thickness and the clarity of the varve structures, it is possible to infer the  
626 deposition mechanism for each layer and the season in which they were deposited.

627  
628 The early spring layers are interpreted to be deposited during the river and lake ice break-  
629 up and disintegration period, when erosion and resuspension of fine-grained sediments are  
630 initiated but still low. Available Landsat-8 images of Grand Lake covering the 1983-2018  
631 period (courtesy of the U.S. Geological Survey) shows that Grand Lake ice cover starts to  
632 melt at the Naskaupi and Beaver River mouths. This ice melting pattern creates open bays  
633 where drifting floating ice melts, thus depositing ice-rafted debris (Lamoureux 1999, 2004)  
634 as observed in the early spring layer facies. The overlying detrital layers are interpreted as  
635 flood-induced turbidites deposited at the lake bottom during the open-water season. High  
636 energy sediment-laden river flows produce hyperpycnal flows allowing silt and sand-size  
637 sediments to reach the cored sites (Cockburn and Lamoureux, 2008). The sharp contact  
638 boundary between the early spring layer and the detrital layer at the top part of the early  
639 spring layer supports the hypothesis that the detrital layers originate from underflows  
640 (Mangili et al., 2005). The sediment waves on the Naskaupi and Beaver river delta slopes  
641 (Trottier et al., 2020) (Fig. 1b, c) also indicate significant downstream sediment transport  
642 by supercritical density flows (Normandeau et al., 2016). The thick and grading upward  
643 basal part of the detrital layers are deposited during the high spring discharge period  
644 generated by snowmelt runoffs. The lack of erosion marks between the early spring layer  
645 and the detrital layer and the incorporation of rare cohesive sediment clasts within the  
646 detrital layer suggests that erosion of the underlying early spring layers occurs in more

647 proximal and energetic settings. Three observations justify the combination of varve  
648 measurements from the 3 coring sites : 1) the sedimentary processes inferred from the  
649 observation of thin-sections, the high resolution bathymetric and the sub-bottom surveys  
650 are similar; (2) the similarity of the varve facies and properties for each single year at the  
651 3 different sites suggest a sedimentary pattern devoid of disturbances due to local factors;  
652 (3) Grains-size differences are too subtle to infer different sedimentary processes and  
653 environments. The upper part of varve structure in core NAS-1 show the most perceptible  
654 different after 1972 (see discussion below). In spring, river discharge reaches its annual  
655 peaks and sediment transport capacities that are then no longer reached during the rest of  
656 the summer and autumn (Fig. 2, 3c, 11). However, the presence of thin coarser intercalated  
657 sub-layers in the upper part of the detrital layer indicates that some rainfall events, as  
658 observed in Fig. 11 (i.e., 1983, 1987, 1992, 1999) also contribute to deposition of sediments  
659 in this layer. The overlying autumn and winter layer resulted from the settling and  
660 flocculation of fine particles in non-turbulent condition from fall through the onset of lake  
661 ice, forming a typical clay cap.



662

663 Figure 11. Qualitative comparison between NAS-1A varves from thin-sections (delimited by the black bars)  
 664 with the hydrographs of the Naskaupi River. Observed annual  $Q$ -mean and  $Q$ -max as well as the timing and  
 665 rise time of the peak spring discharge are shown. Black dotted lines represent the discharge threshold of  
 666  $\sim 125 \text{ m}^3 \cdot \text{sec}^{-1}$ . (1999, 1992, 1986, 1983) Strong spring floods associated with thick coarse varves. (1995,  
 667 1987) Low spring floods associated with thin varves. (1999, 1992, 1987, 1983) Coarser intercalated sub-  
 668 layers in the upper part of the detrital layer linked with summer and autumn high-discharge events. (1986)  
 669 Strong spring flood with a low summer and autumn flow associated to a varve without substructure. Thin-  
 670 sections are overlain by iron (Fe: yellow line), strontium (Sr: blue line), and calcium (Ca: black line) relative  
 671 intensities. See Fig. 5 for thin-sections locations.

672 **5.2 Anthropogenic influences on recent sedimentation**

673 Anthropogenic environmental impacts on watersheds can be preserved in varved lake  
674 sediments (Zolitschka et al., 2015; Saarni et al., 2016; Czymzik et al., 2018). Changes  
675 observed in physical parameters of the varves deposited pre- and post-1971 at the NAS  
676 sites suggest that the effect of the dyke system on the Naskaupi River sediment inputs is  
677 perceptible in the Grand Lake varved sequence. The well-developed layers of varves  
678 deposited prior to 1972 from sites NAS-1 (Fig. 6b) and NAS-2, and the similarity between  
679 TVT and DLT values and variations among all sites over the 1856-1971 period (Fig. 6d)  
680 indicate that before the Naskaupi River diversion, seasonal sedimentation cycles appeared  
681 to have reached a relative state of equilibrium. The reduction of nearly half of the area of  
682 the Naskaupi River watershed due to its diversion in April 1971, reduced the water inflows  
683 and changed the base level of the downstream river system. The rapid base level fall must  
684 have triggered modifications of the fluvial dynamics from late-spring to winter 1971 (i.e.,  
685 channel incision, bank destabilization, and upstream knickpoint migration), likely  
686 increasing the availability of sediments in the river system. The Naskaupi River  
687 spring/summer/autumn flood(s) of 1972 have then remobilized and transported a large  
688 amount of newly available floodplain sediments. This major sediment discharge plunged  
689 in Grand Lake and extended as hyperpycnal flow in the axis of the Naskaupi River  
690 depositing a thick and coarse-grained turbidite following the lake bathymetry. This 1972  
691 marker bed suggests that the Naskaupi River diversion had an impact on sedimentation at  
692 sites NAS-1 and NAS-2.

693  
694 The thin early spring layers free of ice-rafted debris in varve post-1971 of core NAS-1 (Fig.  
695 5a, 11) and NAS-2 indicate the decrease of the capacity of early spring discharge to  
696 transport fine sediments and its ability to float ice to Grand Lake (see section 4.1) due to  
697 the reduction in water supplies caused by the Naskaupi River diversion. The increase in  
698 thickness and particle size values of the detrital layers post-1971 in core NAS-1 (Fig. 5a,  
699 6b, 7b, 11) suggest that the diversion has affected sedimentation at this site over time.  
700 During the 1972-2016 period, the river floodplain morphology must have been in a re-  
701 equilibration phase favourable to erosion, sediment transport, and deposition of thicker and  
702 coarser detrital layers. Since the river diversion, detrital layers at NAS-1 site appears to

- Déplacé (insertion) [1]
- Supprimé: that
- Supprimé: decreases along with the decrease in
- Supprimé: varves deposited
- Supprimé: 6d
- Supprimé: /e
- Supprimé: varves
- Supprimé: on the Naskaupi River delta slope
- Supprimé: sedimentation

711 have become more sensitive to maximum **spring** discharges variations, than mean annual  
712 discharges. The sensitivity of the more proximal NAS-1 site to Naskaupi River extreme  
713 discharges variability may partly explain why better results are obtained without the 1972-  
714 2016 period to reconstruct Q-mean and by keeping this period to the Q-max reconstruction.  
715 The negative correlation between P99D<sub>0</sub> of the core NAS-1 and the timing and rise time of  
716 spring discharge (Table 3) also demonstrate reactivity to spring entrainment energy  
717 conditions at this site. The distal NAS-2 site shows that post-1971, sedimentation seems to  
718 have slightly lost sensitivity to river discharge, and that sediment input continued to decline  
719 at the beginning of the deep lake basin. The increase in sediment input at the site NAS-1  
720 after 1971, contrasts with the decrease in sediment input at the site NAS-2. This recent  
721 difference in sedimentation between these two sites could be explained by the increased  
722 availability of sediments for erosion in the floodplain, which would have favoured the  
723 accumulation of additional sediments mainly on the front of the delta (NAS-1), while the  
724 reduction in maximum discharges due to a smaller watershed would have resulted in a  
725 decrease in the river's transport capacity to the site NAS-2.

Supprimé: in spring

Déplacé vers le haut [1]: The thin early spring layers free of ice-rafted debris in varve post-1971 of core NAS-1 (Fig. 5a, 11) and NAS-2 indicate that the capacity of early spring discharge to transport fine sediments and its ability to float ice to Grand Lake decreases along with the decrease in water supplies.

726  
727 It is **indeed** tempting to link the decrease of varve thickness in core NAS-2 over the 1972-  
728 2016 period with the discharge reduction due to the river diversion. However, similarities  
729 with core BEA-1, a site devoid of anthropogenic perturbations (unaffected by the Naskaupi  
730 River diversion) which also shows a decline in varve thickness, suggest that this decrease  
731 can potentially be due to natural hydro-climatic conditions. The observed Naskaupi River  
732 Q-mean series also show a decrease on the 1978-2011 period. Indeed, because of the distant  
733 location of site BEA-1 from the Naskaupi River mouth, the diversion is most likely not  
734 responsible for the decrease of varve thickness in this sector. Moreover, it is quite unlikely  
735 that the sedimentary input from the Naskaupi River contributed to sediment accumulation  
736 at the mouth of the Beaver River. The absence of any traces of the 1972 marker bed at the  
737 Beaver River mouth (BEA-1) supports this hypothesis. Furthermore, the thickness decrease  
738 observed in BEA-1 began after ~1920 (Fig. 6a), which is before the 1971 diversion.

739  
740 Anthropogenic modification of the Naskaupi River watershed makes it challenging to  
741 discuss natural hydroclimate-related variations before and after 1971. Some caution should

749 be applied when comparing pre- to post 1972 reconstructions, given the changes in  
750 watershed conditions that happened after the construction of the system of dykes. There is  
751 no instrumental data available for the Naskaupi River watershed before 1971 to confirm  
752 that the calibration model post-diversion (1978-2011) is similarly robust for the preceding  
753 period. The river diversion affected the Naskaupi River sedimentation dynamics but did  
754 not modify it drastically. Despite the observed post-diversion changes in varves' physical  
755 parameters in cores NAS-1 and NAS-2, which are however moderate, the varves still  
756 responded directly to variations in river discharge. In addition, the part of the watershed  
757 that has been diverted is an area composed mainly of lakes, which are not very  
758 hydrologically reactive.

### 759 **5.3 The hydrological signal in the varve record**

760 The significant correlations between continuous varve thickness and particle size  
761 measurements with instrumental hydrological variables (Tab. 3) show that Grand Lake  
762 varved sediments are reliable proxies to reconstruct past hydrologic conditions through  
763 time at the annual to seasonal scale. The thick and/or coarse-grained varves correspond  
764 well to years of high river discharges, whereas thin and/or fine-grained varves are related  
765 with years of low discharge. Moreover, figure 11 clearly demonstrates how Grand Lake  
766 varve record can be exploited to examine the interaction between meteorological  
767 conditions and rivers discharge at an inter-seasonal scale, which is a temporal resolution  
768 rarely obtained with natural proxies.

769

770 Data from the 3 sites were combined in order to better capture the regional **hydrological**  
771 signal and to somehow attenuate the noise that is inherent from the analysis of a single core  
772 in a very large lake. A single core will be more sensitive to local specificities and is  
773 probably less representative of the entire hydrogram. The Beaver and the Naskaupi Rivers  
774 have adjacent catchments that share the same climatological and geological characteristics,  
775 while the Beaver River's catchment is devoid of anthropogenic modifications. The  
776 combination of varve parameters from different coring sites with distinct sediment sources  
777 (Fig. 1b) improved the correlations with local and regional hydrological variables (Tab. 3)  
778 and thereby the reconstructions (Fig. 8, 9). By integrating the core BEA into the combined

Supprimé: hydroclimatic

780 data, it allows to capture the hydrological signal from a larger region (Nakaupi + Beaver  
781 watersheds) and it helps to capture the natural hydrological signal in our combined series  
782 used for reconstructions.

783

784 As demonstrated by previous studies on varved sediments, the use of both varve thickness  
785 and particle size analysis allows for a more specific investigation of the range of  
786 hydroclimate conditions recorded within varves (Francus et al., 2002; Cockburn and  
787 Lamoureux, 2008; Lapointe et al., 2012). For Grand Lake, the combined DLT is found to  
788 be the best proxy to reconstruct all hydrological events occurring throughout the year (Q-  
789 mean). DLT series are better at predicting Q-mean because the early spring layers and  
790 autumn and winter layers thickness are more variable and are included in the TVT  
791 measurements. This variability can be linked to specific climatic and geomorphological  
792 parameters such as the duration of ice cover on Grand Lake and the Naskaupi River ice  
793 breakup processes which induce noise in the hydrologic signal contained in TVT series.  
794 The combined P99D<sub>0</sub> yields the strongest correlation in our dataset (Tab. 3) and is the best  
795 proxy to reconstruct maximum annual discharges (Q-max). This result is logical because  
796 the peak discharge is controlling the competence of the river and consequently the size of  
797 the particles that can be transported. Moreover, this indicator is not sensitive to sediment  
798 compaction, which may affect other proxies based on thickness.

799

800 The significant positive correlations between varve physical parameters and Q-max and Q-  
801 nival (Tab. 3) demonstrate that Grand Lake varve predominantly reflects spring discharge  
802 conditions (e.g., Ojala and Alenius 2005; Lamoureux et al., 2006; Saarni et al., 2016;  
803 Czymzik et al., 2018), which is the major component of the regional streamflow regimes  
804 classified as nival (snowmelt-dominated) (Bonsal et al., 2019). In boreal regions, the  
805 intensity and length of spring floods are controlled by the snow accumulation during winter  
806 and by the temperature of the melting period (Hardy et al., 1996; Snowball et al., 1999;  
807 Cockburn and Lamoureux, 2008; Ojala et al., 2013; Saarni et al., 2017). The negative  
808 correlation between P99D<sub>0</sub> of the NAS-1 and the timing and rise time of spring discharge  
809 suggests that early spring flows that increase rapidly are conducive conditions for high  
810 entrainment energy and the deposition of coarser laminations on the distal part of the delta

Supprimé: Snow-Win.

Supprimé: and even Temp-Spring

813 slope (Fig. 11; site NAS-1). The erosion of detrital materials in early spring increases when  
814 the snowmelt runoffs occur on soils that are not yet stabilized and protected by vegetation  
815 (Ojala and Alenius 2005, Czymzik et al., 2018).

816

817 Intercalated sub-layers in the upper part of the detrital layer are interpreted to be produced  
818 by summer or fall rainfall events (Fig. 11). Yet, the significant positive correlations  
819 between varve thickness and Nb-days-SupQ80 suggests that a daily discharge of  $\sim 125 \text{ m}^3\cdot\text{s}^{-1}$   
820 <sup>1</sup> represents an approximate threshold above which the deposition of coarse sediments in  
821 Grand Lake (detrital layers) is more likely to occur (Fig. 11) (e.g., Czymzik et al., 2010,  
822 Kämpf et al., 2014). According to the instrumental data (Fig. 2, 11), such a discharge can  
823 be generated during the summer/autumn period, confirming that rainfall events can indeed  
824 be triggering the deposition of thin intercalated sub-layers observed in the upper part of the  
825 detrital layers (Fig. 11).

826

827 The comparison between the Naskaupi River hydrological variables and other Labrador  
828 hydrometric stations (Fig. 3) show that a coherent regional hydrological pattern exists in  
829 the Labrador region. The performed regional Q-mean reconstitution and validation (Fig. 9)  
830 indicated that the Labrador region hydrologic signal is recorded in the Grand Lake varve  
831 sequence. The local and regional Q-mean reconstructed from the combined DLT series  
832 (without the NAS-1 1972-2016 period) suggest a statistically significant decreasing trend  
833 in mean annual discharge during the last 90 years. Naskaupi River Q-mean and Q-max  
834 reconstructions based on both varve series and rainfall-runoff modelling revealed high  
835 value periods from 1975 to 1985 and 1995 to 2005, and low values from 1986 to 1994 and  
836 2006 to 2016 (Fig. 10). These results agree with the downward trend of the annual  
837 streamflow observed in eastern Canada during the 20<sup>th</sup> century in other studies and also  
838 with the reported higher river discharges from 1970 to 1979 and 1990 to 2007, and lower  
839 discharges from 1980 to 1989 (Zhang et al. 2001; Sveinsson et al., 2008; Jandhyala et al.,  
840 2009; Déry et al., 2009; Mortsch et al., 2015; Dinis et al., 2019).

841

842 In addition to providing a new high-quality varved record in eastern Canada, this research  
843 highlights the complementarity between palaeohydrological reconstructions extracted

**Supprimé:** However, there is non-significant low correlations between varves thickness and Ptot-Annual/Ptot-Sum (not shown) suggesting that rainfalls contributions to TVT remain small. These rainfall events have no contribution to P99D<sub>0</sub> because the coarsest particles are found at the base of the detrital layers.

**Supprimé:** -climatic

851 from clastic varved sediments and rainfall-runoff modelling. Both methods independently  
852 offer a similar, yet robust, centennial perspective on river discharge variability in an  
853 important region for the economic and sustainable development of water resources in  
854 Canada. Reconstructed long-term mean and maximum annual river discharges series  
855 provide valuable quantitative information particularly for water supply management for  
856 hydropower generation and the estimation of flood and drought hazards. The varved  
857 sediment of Grand Lake also allows documenting the effect of dyke systems on the  
858 downstream sediment transport dynamic into a watershed and its implication for  
859 palaeohydrological reconstruction. Further investigation of the impacts of the Naskaupi  
860 watershed reduction on sediment transport could help better refine these reconstructions.  
861 Future work in Grand Lake should be directed towards the high-resolution analysis of long  
862 sediment cores in order to produce longer reconstructions. The Grand Lake deeper varved  
863 sequence potentially recorded the hydro-climatic variability that occurred during the Late  
864 Holocene in region sensitive to the North Atlantic climate, allowing interesting prospects  
865 into large-scale atmospheric and oceanic modes of variability.

866

## 867 **6. Conclusions**

868 The great depth of Grand Lake, the availability of fine sediments along its tributaries, and  
869 its important seasonal river inflow have favoured the formation and preservation of fluvial  
870 clastic laminated sediments. By using a new varved record in eastern Canada and a rainfall-  
871 runoff modelling approach, this paper provides a better understanding of the recording of  
872 hydrological conditions in large and deep boreal lakes and allows extending the discharge  
873 series beyond the instrumental period as well as the spatial coverage of the rare annual  
874 palaeohydrological proxies in North America. The key results of this study are:

- 875 • The annual character of the 160 years-long lamination sequence has been confirmed.  
876 Each varve, composed of an early spring layer, a summer/autumn detrital layer and an  
877 autumn and winter layer, represents one hydrological year.
- 878 • Grand Lake varve formation is mainly related to the largest hydrological event of the  
879 year, the spring discharge, with contributions from summer and autumn rainfall events.
- 880 • Two hydrological parameters, the Naskaupi river Q-mean and Q-max annual  
881 discharges, are robustly reconstructed from two independent varves physical

Supprimé: climatic

Supprimé: hydrological

Supprimé: minor

885 parameters, i.e., the detrital layer thickness (DLT) and grain size (P99D<sub>0</sub>) respectively,  
886 over the 1856-2016 period. The reconstructed Q-mean series suggest that high Q-mean  
887 years occurred during the 1920-1960 period and a decrease in Q-mean takes place  
888 during the second half of the 20<sup>th</sup> century.

- 889 • The same two hydrological parameters (Q-mean and Q-max), were also reconstructed  
890 using the ANATEM rainfall-runoff modelling. ANATEM discharges series show  
891 similarities with reconstructions based on the varved series, which support the  
892 reliability of the two independent reconstruction approaches.
- 893 • The statistically significant relation between combined DLT series and the observed  
894 Labrador region Q-mean series, extracted from five watersheds of different size and  
895 location, demonstrates that Grand Lake varved sequence can also be used as a proxy of  
896 regional river discharges conditions.
- 897 • The effects of Naskaupi River dyking in 1971 are clearly visible in the sedimentary  
898 record and affected sedimentary patterns afterwards. While this event makes the  
899 hydroclimatic reconstruction trickier, it remains that the outstanding quality of this  
900 varved sequence provides one of the best hydroclimatic reconstruction from a  
901 sedimentary record, with Pearson correlation coefficients up to  $r = 0.75$ .
- 902

903 **Data availability**

904 The data set used in this study will be available on the PANGAEA database.

905

906 **Author contributions**

907 This study is part of AGP's thesis under the supervision of PF and PL. AT and PL provided  
908 geophysical data (Fig. 1b, c) and useful information on the morpho-stratigraphical  
909 framework of Grand Lake. AGP and DF conducted the coring fieldtrip. AGP and PB  
910 collected instrumental data. PB calculated hydrological variables from instrumental data  
911 (Fig. 3) and performed the rainfall-runoff modelling. HD and AGP adapted the code used  
912 to establish the relationship between the varve parameters and the instrumental data and  
913 for the regression model. AGP performed most of the data analysis, wrote the manuscript  
914 and created the figures with contributions from PF and PB. All authors provided valuable  
915 feedback and contributed to the improvement of the manuscript.

916

917 **Competing interests**

918 The author Pierre Francus is a member of the editorial board of the journal.

919

920 **Acknowledgments**

921 This research was financially supported by NSERC-Ouranos-Hydro-Québec-Hydro-  
922 Manitoba through a CRD grant to P.F. and P.L. (PERSISTANCE project, É. Boucher et  
923 al.). This work was also supported by the FRQNT through a doctoral (B2X) research  
924 scholarship to A.G.P. and by the MOPGA Short Stay program grant at Université Côte  
925 d'Azur, Nice, France to A.G.P and P.B. A financial support for the fieldwork campaign at  
926 Grand Lake was provided by POLAR through the NSTP program to A.G.P. The authors  
927 are grateful to Arnaud De Coninck, David Deligny and Louis-Frédéric Daigle for their  
928 participation during fieldwork, laboratory and helpful discussions. We greatly thank  
929 Wanda and Dave Blake from North West River for their guiding experience and  
930 accommodation at Grand Lake. We thank the Labrador Institute at North West River for  
931 the use of their facility during fieldwork. We want to thank Stéphane Ferré from the Micro-  
932 Geoarchaeology Laboratory of the Center for Northern Studies (CEN) in Québec, QC,  
933 Canada, for the production of the high-quality thin-sections used in this study. We would

Supprimé: -climatic

935 also like to thank the three reviewers for their constructive review of this article. Finally,  
936 many thanks to Monique Gagnon, Charles Smith and Clarence Gagnon for reviewing the  
937 English of an earlier version of the manuscript.

938 **References**

- 939 Amann, B., Szidat, S., and Grosjean, M.: A millennial-long record of warm season  
940 precipitation and flood frequency for the North-western Alps inferred from varved lake  
941 sediments: implications for the future, *Quaternary. Sci. Rev.*, 115, 89-100,  
942 <https://doi.org/10.1016/j.quascirev.2015.03.002>, 2015.
- 943
- 944 Anderson, T.: *Rivers of Labrador*, Canadian Special Publication of Fisheries and Aquatic  
945 Sciences 81, Ottawa, Ontario, 1985.
- 946
- 947 Appleby, P. and Oldfield, F.: The calculation of lead-210 dates assuming a constant rate of  
948 supply of unsupported <sup>210</sup>Pb to the sediment, *Catena*, 5, 1-8,  
949 [https://doi.org/10.1016/S0341-8162\(78\)80002-2](https://doi.org/10.1016/S0341-8162(78)80002-2), 1978.
- 950
- 951 Bégin, C., Gingras, M., Savard, M. M., Marion, J., Nicault, A., and Bégin, Y.: Assessing  
952 tree-ring carbon and oxygen stable isotopes for climate reconstruction in the Canadian  
953 northeastern boreal forest, *Palaeogeography, Palaeoclimatology, Palaeoecology*, 423, 91-  
954 101, <https://doi.org/10.1016/j.palaeo.2015.01.021>, 2015.
- 955
- 956 Bégin, Y., Nicault, A., Bégin, C., Savard, M. M., Arseneault, D., Berninger, F., Guiot, J.,  
957 Boreux, J.-J., and Perreault, L.: Analyse dendrochronologique des variations passées du  
958 régime hydro climatique au complexe de la grande rivière dans le Nord du Québec, *La*  
959 *Houille Blanche*, 2007. 70-77, <https://doi.org/10.1051/lhb:2007085>, 2007.
- 960
- 961 Bonsal, B.R., Peters, D.L., Seglenieks, F., Rivera, A., and Berg, A.: Changes in freshwater  
962 availability across Canada; Chapter 6 in *Canada's Changing Climate Report*, (ed.) E. Bush  
963 and D.S. Lemmen; Government of Canada, Ottawa, Ontario, 2019.
- 964
- 965 Boucher, E., Nicault, A., Arseneault, D., Bégin, Y., and Karami, M. P.: Decadal Variations  
966 in Eastern Canada's Taiga Wood Biomass Production Forced by Ocean-Atmosphere  
967 Interactions, *Sci. Rep. Uk.*, 7, 1-13, <https://doi.org/10.1038/s41598-017-02580-9>, 2017.
- 968
- 969 Boucher, É., Ouarda, T. B., Bégin, Y., and Nicault, A.: Spring flood reconstruction from  
970 continuous and discrete tree ring series, *Water. Resour. Res.*, 47,  
971 <https://doi.org/10.1029/2010WR010131>, 2011.
- 972
- 973 Briffa, K., Jones, P., Pilcher, J., and Hughes, M.: Reconstructing summer temperatures in  
974 northern Fennoscandia back to AD 1700 using tree-ring data from Scots pine, *Arct.*  
975 *Antartic. Alp. Research.*, 20, 385-394, <https://doi.org/10.1080/00040851.1988.12002691>,  
976 1988.
- 977

978 Brigode, P., Brissette, F., Nicault, A., Perreault, L., Kuentz, A., Mathevet, T., and Gailhard,  
979 J.: Streamflow variability over the 1881–2011 period in northern Québec: comparison of  
980 hydrological reconstructions based on tree rings and geopotential height field reanalysis,  
981 *Clim. Past*, 12, 1785-1804, <https://doi.org/10.5194/cp-12-1785-2016>, 2016.

982

983 Cherry, J. E., Knapp, C., Trainor, S., Ray, A. J., Tedesche, M., and Walker, S.: Planning  
984 for climate change impacts on hydropower in the Far North, *Hydrol. Earth Syst. Sci.*, 21,  
985 133, <https://doi.org/10.5194/hess-21-133-2017>, 2017.

986

987 Cockburn, J. M. and Lamoureux, S. F.: Inflow and lake controls on short-term mass  
988 accumulation and sedimentary particle size in a High Arctic lake: implications for  
989 interpreting varved lacustrine sedimentary records, *J. Paleolimnol.*, 40, 923-942,  
990 <https://doi.org/10.1007/s10933-008-9207-5>, 2008.

991

992 Collins, M., Knutti, R., Arblaster, J., Dufresne, J-L., Fichefet, T., Friedlingstein, P., Gao,  
993 X., Gutowski, W. J., Johns, T., Krinner, G., Shongwe, M., Tebaldi, C., Weaver, A. J.,  
994 Wehner, M. F., Allen, M. R., Andrews, T., Beyerle, U., Bitz, C. M., Bony, S., & Booth, B.  
995 B. B.: Long-term climate change: projections, commitments and irreversibility, In: *Climate  
996 Change 2013 - The Physical Science Basis, Contribution of Working Group I to the Fifth  
997 Assessment Report of the Intergovernmental Panel on Climate Change*, Intergovernmental  
998 Panel on Climate Change, Cambridge University Press, 1029-1136, 2013.

999

1000 Compo, G. P., Whitaker, J. S., Sardeshmukh, P. D., Matsui, N., Allan, R. J., Yin, X.,  
1001 Gleason, B. E., Vose, R. S., Rutledge, G., and Bessemoulin, P.: The twentieth century  
1002 reanalysis project, *Q J R Meteorol Soc*, 137, 1-28, <https://doi.org/10.1002/qj.776>, 2011.

1003

1004 Cook, E. R., Meko, D. M., Stahle, D. W., and Cleaveland, M. K.: Drought reconstructions  
1005 for the continental United States, *J. Clim.*, 12, 1145-1162, [https://doi.org/10.1175/1520-0442\(1999\)012%3C1145:DRFTCU%3E2.0.CO;2](https://doi.org/10.1175/1520-0442(1999)012%3C1145:DRFTCU%3E2.0.CO;2), 1999.

1006

1007

1008 Coron, L., Thirel, G., Delaigue, O., Perrin, C., and Andréassian, V.: The suite of lumped  
1009 GR hydrological models in an R package, *Environmental Modelling & Software*, 94, 166-  
1010 171, <https://doi.org/10.1016/j.envsoft.2017.05.002>, 2017.

1011

1012 Croudace, I. W., Rindby, A., and Rothwell, R. G.: ITRAX: description and evaluation of a  
1013 new multi-function X-ray core scanner, Geological Society, London, Special Publications,  
1014 267, 51-63, <https://doi.org/10.1144/GSL.SP.2006.267.01.04>, 2006.

1015

1016 Cuvén, S., Francus, P., and Lamoureux, S.: Mid to Late Holocene hydroclimatic and  
1017 geochemical records from the varved sediments of East Lake, Cape Bounty, Canadian High

1018 Arctic, Quaternary. Sci. Rev., 30, 2651-2665,  
1019 <https://doi.org/10.1016/j.quascirev.2011.05.019>, 2011.  
1020  
1021 Cuvén, S., Francus, P., and Lamoureux, S. F.: Estimation of grain size variability with  
1022 micro X-ray fluorescence in laminated lacustrine sediments, Cape Bounty, Canadian High  
1023 Arctic, *J. Paleolimnol.*, 44, 803-817, <https://doi.org/10.1007/s10933-010-9453-1>, 2010.  
1024  
1025 Czymzik, M., Dulski, P., Plessen, B., Von Grafenstein, U., Naumann, R., and Brauer, A.:  
1026 A 450 year record of spring-summer flood layers in annually laminated sediments from  
1027 Lake Ammersee (southern Germany), *Water. Resour. Res.*, 46,  
1028 <https://doi.org/10.1029/2009WR008360>, 2010.  
1029  
1030 Czymzik, M., Haltia, E., Saarni, S., Saarinen, T., and Brauer, A.: Differential North  
1031 Atlantic control of winter hydroclimate in late Holocene varved sediments of Lake  
1032 Kortejärvi, eastern Finland, *Boreas*, 47, 926-937, <https://doi.org/10.1111/bor.12315>, 2018.  
1033  
1034 D'Arrigo, R., Buckley, B., Kaplan, S., and Woollett, J.: Interannual to multidecadal modes  
1035 of Labrador climate variability inferred from tree rings, *Clim. Dynam.*, 20, 219-228,  
1036 <https://doi.org/10.1007/s00382-002-0275-3>, 2003.  
1037  
1038 Déry, S. J. and Wood, E. F.: Decreasing river discharge in northern Canada, *Geophys. Res.*  
1039 *Lett.*, 32, <https://doi.org/10.1029/2005GL022845>, 2005.  
1040  
1041 Dinis, L., Bégin, C., Savard, M. M., Marion, J., Brigode, P., and Alvarez, C.: Tree-ring  
1042 stable isotopes for regional discharge reconstruction in eastern Labrador and  
1043 teleconnection with the Arctic Oscillation, *Clim. Dynam.*, 53, 3625-3640,  
1044 <https://doi.org/10.1007/s00382-019-04731-2>, 2019.  
1045  
1046 Fitzhugh, W.: Environmental Approaches to the Prehistory of the North, *Journal of the*  
1047 *Washington Academy of Sciences*, 1973. 39-53, 1973.  
1048  
1049 Francus, P.: An image-analysis technique to measure grain-size variation in thin sections  
1050 of soft clastic sediments, *Sedimentary Geology*, 121, 289-298,  
1051 [https://doi.org/10.1016/S0037-0738\(98\)00078-5](https://doi.org/10.1016/S0037-0738(98)00078-5), 1998.  
1052  
1053 Francus, P., Bradley, R. S., Abbott, M. B., Patridge, W., and Keimig, F.: Paleoclimate  
1054 studies of minerogenic sediments using annually resolved textural parameters, *Geophys.*  
1055 *Res. Lett.*, 29, 59-51-59-54, <https://doi.org/10.1029/2002GL015082>, 2002.  
1056

1057 Francus, P. and Cosby, C. A.: Sub-sampling unconsolidated sediments: A solution for the  
1058 preparation of undisturbed thin-sections from clay-rich sediments, *J. Paleolimnol*, 26, 323-  
1059 326, <https://doi.org/10.1023/A:1017572602692>, 2001.  
1060  
1061 Francus, P. and Karabanov, E.: A computer-assisted thin-section study of Lake Baikal  
1062 sediments: a tool for understanding sedimentary processes and deciphering their climatic  
1063 signal, *Int. J. Earth. Sci.*, 89, 260-267, <https://doi.org/10.1007/s005319900064>, 2000.  
1064  
1065 Francus, P., Keimig, F., and Besonen, M.: An algorithm to aid varve counting and  
1066 measurement from thin-sections, *Journal of Paleolimnology*, 28, 283-286,  
1067 <https://doi.org/10.1023/A:1021624415920>, 2002.  
1068  
1069 Francus, P. and Nobert, P.: An integrated computer system to acquire, process, measure  
1070 and store images of laminated sediments, In 4th International limnogeology congress,  
1071 Barcelona, July, 2007.  
1072  
1073 Fulton, R. J. and Ferguson, J.: *Surficial Geology Cartwright: Labrador, Newfoundland,*  
1074 *Commission, Department of Energy, Mines and Resources*, 1986.  
1075  
1076 Gilbert, R. and Desloges, J. R.: Late glacial and Holocene sedimentary environments of  
1077 Quesnel Lake, British Columbia, *Geomorphology*, 179, 186-196,  
1078 <https://doi.org/10.1016/j.geomorph.2012.08.010>, 2012.  
1079  
1080 Gupta, H. V., Kling, H., Yilmaz, K. K., and Martinez, G. F.: Decomposition of the mean  
1081 squared error and NSE performance criteria: Implications for improving hydrological  
1082 modelling, *J. Hydrol.*, 377, 80-91, <https://doi.org/10.1016/j.jhydrol.2009.08.003>, 2009.  
1083  
1084 Hardy, D. R., Bradley, R. S., and Zolitschka, B.: The climatic signal in varved sediments  
1085 from Lake C2, northern Ellesmere Island, Canada, *J. Paleolimnol.*, 16, 227-238,  
1086 <https://doi.org/10.1007/BF00176938>, 1996.  
1087  
1088 Heideman, M., Menounos, B., and Clague, J. J.: An 825-year long varve record from  
1089 Lillooet Lake, British Columbia, and its potential as a flood proxy, *Quaternary. Sci. Rev.*,  
1090 126, 158-174, <https://doi.org/10.1016/j.quascirev.2015.08.017>, 2015.  
1091  
1092 Jandhyala, V. K., Liu, P., and Fotopoulos, S. B.: River stream flows in the northern Québec  
1093 Labrador region: A multivariate change point analysis via maximum likelihood, *Water.*  
1094 *Resour. Res.*, 45, <https://doi.org/10.1029/2007WR006499>, 2009.  
1095  
1096 Kämpf, L., Brauer, A., Swierczynski, T., Czymzik, M., Mueller, P., and Dulski, P.:  
1097 Processes of flood-triggered detrital layer deposition in the varved Lake Mondsee sediment

1098 record revealed by a dual calibration approach, *Journal of Quaternary Science*, 29, 475-  
1099 486, <https://doi.org/10.1002/jqs.2721>, 2014.  
1100  
1101 Kaufman, C. A., Lamoureux, S. F., and Kaufman, D. S.: Long-term river discharge and  
1102 multidecadal climate variability inferred from varved sediments, southwest Alaska, *Quat.*  
1103 *Res.*, 76, 1-9, <https://doi.org/10.1016/j.yqres.2011.04.005>, 2011.  
1104  
1105 Kuentz, A., Mathevet, T., Gailhard, J., and Hingray, B.: Building long-term and high  
1106 spatio-temporal resolution precipitation and air temperature reanalyses by mixing local  
1107 observations and global atmospheric reanalyses: the ANATEM model, *Hydrol. Earth Syst.*  
1108 *Sci.*, 19, 2717-2736, <https://doi.org/10.5194/hess-19-2717-2015>, 2015.  
1109  
1110 Kylander, M. E., Ampel, L., Wohlfarth, B., and Veres, D.: High-resolution X-ray  
1111 fluorescence core scanning analysis of Les Echets (France) sedimentary sequence: new  
1112 insights from chemical proxies, *J. Quat. Sci.*, 26, 109-117,  
1113 <https://doi.org/10.1002/jqs.1438>, 2011.  
1114  
1115 Lamoureux, S.: Five centuries of interannual sediment yield and rainfall-induced erosion  
1116 in the Canadian High Arctic recorded in lacustrine varves, *Water. Resour. Res.*, 36, 309-  
1117 318, <https://doi.org/10.1029/1999WR900271>, 2000.  
1118  
1119 Lamoureux, S. F.: Embedding unfrozen lake sediments for thin section preparation, *J.*  
1120 *Paleolimnol.*, 10, 141-146, <https://doi.org/10.1007/BF00682510>, 1994.  
1121  
1122 Lamoureux, S. F., Stewart, K. A., Forbes, A. C., and Fortin, D.: Multidecadal variations  
1123 and decline in spring discharge in the Canadian middle Arctic since 1550 AD, *Geophys.*  
1124 *Res. Lett.*, 33, <https://doi.org/10.1029/2005GL024942>, 2006.  
1125  
1126 Lapointe, F., Francus, P., Lamoureux, S. F., Saïd, M., and Cuvén, S.: 1750 years of large  
1127 rainfall events inferred from particle size at East Lake, Cape Bounty, Melville Island,  
1128 Canada, *J. paleolimnol.*, 48, 159-173, <https://doi.org/10.1007/s10933-012-9611-8>, 2012.  
1129  
1130 Linderholm, H. W., Nicolle, M., Francus, P., Gajewski, K., Helama, S., Korhola, A.,  
1131 Solomina, O., Yu, Z., Zhang, P., D'Andrea, W. J., Debret, M., Divine, D. V., Gunnarson,  
1132 B. E., Loader, N. J., Massei, N., Seftigen, K., Thomas, E. K., Werner, J., Andersson, S.,  
1133 Berntsson, A., Luoto, T. P., Nevalainen, L., Saarni, S., and Väiliranta, M.: Arctic  
1134 hydroclimate variability during the last 2000 years: current understanding and research  
1135 challenges, *Clim. Past*, 14, 473–514, <https://doi.org/10.5194/cp-14-473-2018>, 2018.  
1136

1137 Ljungqvist, F. C., Krusic, P. J., Sundqvist, H. S., Zorita, E., Brattström, G., and Frank, D.:  
1138 Northern Hemisphere hydroclimate variability over the past twelve centuries, *Nature*, 532,  
1139 94-98, <https://doi.org/10.1038/nature17418>, 2016.  
1140  
1141 Mangili, C., Brauer, A., Moscariello, A., and Naumann, R.: Microfacies of detrital event  
1142 layers deposited in Quaternary varved lake sediments of the Piànico-Sèllere Basin  
1143 (northern Italy), *Sedimentology*, 52, 927-943, [https://doi.org/10.1111/j.1365-  
1144 3091.2005.00717.x](https://doi.org/10.1111/j.1365-3091.2005.00717.x), 2005.  
1145  
1146 Mortsch, L., Cohen, S., and Koshida, G.: Climate and water availability indicators in  
1147 Canada: Challenges and a way forward. Part II—Historic trends, *Can. Water Resour. J.*, 40,  
1148 146-159, <https://doi.org/10.1080/07011784.2015.1006024>, 2015.  
1149  
1150 Naulier, M., Savard, M. M., Bégin, C., Gennaretti, F., Marion, J., Nicault, A., and Bégin,  
1151 Y.: A millennial summer temperature reconstruction for northeastern Canada using oxygen  
1152 isotopes in subfossil trees, *Clim. Past*, 11, 1153-1164, [https://doi.org/10.5194/cp-11-1153-  
1153 2015](https://doi.org/10.5194/cp-11-1153-2015), 2015.  
1154  
1155 Nicault, A., Boucher, E., Bégin, C., Guiot, J., Marion, J., Perreault, L., Roy, R., Savard, M.  
1156 M., and Bégin, Y.: Hydrological reconstruction from tree-ring multi-proxies over the last  
1157 two centuries at the Caniapiscou Reservoir, northern Québec, Canada, *J. Hydrol.*, 513, 435-  
1158 445, <https://doi.org/10.1016/j.jhydrol.2014.03.054>, 2014.  
1159  
1160 Normandeau, A., Lajeunesse, P., Poiré, A. G., and Francus, P.: Morphological expression  
1161 of bedforms formed by supercritical sediment density flows on four fjord-lake deltas of the  
1162 south-eastern Canadian Shield (Eastern Canada), *Sedimentology*, 63, 2106-2129,  
1163 <https://doi.org/10.1111/sed.12298>, 2016.  
1164  
1165 Notzl, L., Greene, R., and Riley, J.: Labrador Nature Atlas. Vol. II. Ecozones, Ecoregions,  
1166 and Ecodistricts, Nature Conservancy of Canada and Province of Newfoundland and  
1167 Labrador, Toronto, ON, Canada, 2013.  
1168  
1169 Ojala, A. E. and Alenius, T.: 10 000 years of interannual sedimentation recorded in the  
1170 Lake Nautajärvi (Finland) clastic–organic varves, *Palaeogeography, Palaeoclimatology,*  
1171 *Palaeoecology*, 219, 285-302, <https://doi.org/10.1016/j.palaeo.2005.01.002>, 2005.  
1172  
1173 Ojala, A. E., Kosonen, E., Weckström, J., Korkkonen, S., and Korhola, A.: Seasonal  
1174 formation of clastic-biogenic varves: the potential for palaeoenvironmental interpretations,  
1175 *GFF*, 135, 237-247, <https://doi.org/10.1080/11035897.2013.801925>, 2013.  
1176

1177 Oudin, L., Hervieu, F., Michel, C., Perrin, C., Andréassian, V., Anctil, F., and Loumagne,  
1178 C.: Which potential evapotranspiration input for a lumped rainfall–runoff model?: Part 2—  
1179 Towards a simple and efficient potential evapotranspiration model for rainfall–runoff  
1180 modelling, *J. Hydrol.*, 303, 290-306, <https://doi.org/10.1016/j.jhydrol.2004.08.026>, 2005.  
1181  
1182 Perrin, C., Michel, C., and Andréassian, V.: Improvement of a parsimonious model for  
1183 streamflow simulation, *J. Hydrol.*, 279, 275-289, [https://doi.org/10.1016/S0022-  
1184 1694\(03\)00225-7](https://doi.org/10.1016/S0022-1694(03)00225-7), 2003.  
1185  
1186 Rohde, R., Muller, R., Jacobsen, R., Muller, E., Perlmutter, S., Rosenfeld, A., Wurtele, J.,  
1187 Groom, D., and Wickham, C.: A New Estimate of the Average Earth Surface Land  
1188 Temperature Spanning 1753 to 2011, *Geoinfor. Geostat.: An Overview 1: 1, of, 7, 2,*  
1189 <http://dx.doi.org/10.4172/2327-4581.1000101>, 2013.  
1190  
1191 Saarni, S., Lensu, A., Tammelin, M., Haltia, E., and Saarinen, T.: Winter climate signal in  
1192 boreal clastic-biogenic varves: a comprehensive analysis of three varved records from 1890  
1193 to 1990 AD with meteorological and hydrological data from Eastern Finland, *GFF*, 139,  
1194 314-326, <https://doi.org/10.1080/11035897.2017.1389984>, 2017.  
1195  
1196 Saarni, S., Saarinen, T., and Dulski, P.: Between the North Atlantic Oscillation and the  
1197 Siberian High: A 4000-year snow accumulation history inferred from varved lake  
1198 sediments in Finland, *Holocene*, 26, 423-431, <https://doi.org/10.1177/0959683615609747>,  
1199 2016.  
1200  
1201 Schillereff, D. N., Chiverrell, R. C., Macdonald, N., and Hooke, J. M.: Flood stratigraphies  
1202 in lake sediments: A review, *Earth-Sci. Rev.*, 135, 17-37,  
1203 <https://doi.org/10.1016/j.earscirev.2014.03.011>, 2014.  
1204  
1205 Seiller, G., Anctil, F., and Perrin, C.: Multimodel evaluation of twenty lumped hydrological  
1206 models under contrasted climate conditions, *Hydrol. Earth Syst. Sci.*,  
1207 <https://dx.doi.org/10.5194/hess-1116-1171-2012>, 2012.  
1208  
1209 Snowball, I., Sandgren, P., and Petterson, G.: The mineral magnetic properties of an  
1210 annually laminated Holocene lake-sediment sequence in northern Sweden, *Holocene*, 9,  
1211 353-362, <https://doi.org/10.1191/095968399670520633>, 1999.  
1212  
1213 St-Onge, G., Mulder, T., Francus, P., and Long, B.: Chapter two continuous physical  
1214 properties of cored marine sediments, *Developments in marine geology*, 1, 63-98,  
1215 [https://doi.org/10.1016/S1572-5480\(07\)01007-X](https://doi.org/10.1016/S1572-5480(07)01007-X), 2007.  
1216

1217 Stocker, T. F., Qin, D., Plattner, G.-K., Tignor, M. M., Allen, S. K., Boschung, J., Nauels,  
1218 A., Xia, Y., Bex, V., and Midgley, P. M.: Climate change 2013: the physical science basis.  
1219 Contribution of working group I to the fifth assessment report of IPCC the  
1220 intergovernmental panel on climate change. Cambridge University Press,  
1221 <https://dx.doi.org/10.1017/CBO9781107415324>, 2014.  
1222  
1223 Sturm, M.: Origin and composition of clastic varves, In: Schlüchter, C. (Ed.), *Moraines*  
1224 *and Varves: Origin, Genesis, Classification*. A.A. Balkema, Rotterdam, The Netherlands,  
1225 281-285, [https://www.worldcat.org/title/moraines-and-varves-origin-genesis-](https://www.worldcat.org/title/moraines-and-varves-origin-genesis-classification/oclc/5542145)  
1226 [classification/oclc/5542145](https://www.worldcat.org/title/moraines-and-varves-origin-genesis-classification/oclc/5542145), 1979.  
1227  
1228 Sveinsson, O. G., Lall, U., Fortin, V., Perrault, L., Gaudet, J., Zebiak, S., and Kushnir, Y.:  
1229 Forecasting spring reservoir inflows in Churchill Falls basin in Quebec, Canada, *J. Hydrol.*  
1230 *Eng.*, 13, 426-437, [https://dx.doi.org/10.1061/\(Asce\)1084-0699\(2008\)13:6\(426\)](https://dx.doi.org/10.1061/(Asce)1084-0699(2008)13:6(426)), 2008.  
1231  
1232 R Core Team: R: A Language and Environment for Statistical Computing, R Foundation  
1233 for Statistical Computing, Vienna, Austria, <http://www.R-project.org/>, 2019.  
1234  
1235 Tomkins, J. D., Lamoureux, S. F., Antoniades, D., and Vincent, W. F.: Autumn snowfall  
1236 and hydroclimatic variability during the past millennium inferred from the varved  
1237 sediments of meromictic Lake A, northern Ellesmere Island, Canada, *Quat. Res.*, 74, 188-  
1238 198, <https://doi.org/10.1016/j.yqres.2010.06.005>, 2010.  
1239  
1240 Trottier, A. P., Lajeunesse, P., Gagnon-Poiré, A., and Francus, P.: Morphological  
1241 signatures of deglaciation and postglacial sedimentary processes in a deep fjord-lake  
1242 (Grand Lake, Labrador), *Earth Surf. Proc. Land.*, 45, 928-947,  
1243 <https://doi.org/10.1002/esp.4786>, 2020.  
1244  
1245 Valéry, A., Andréassian, V., and Perrin, C.: ‘As simple as possible but not simpler’: What  
1246 is useful in a temperature-based snow-accounting routine? Part 1–Comparison of six snow  
1247 accounting routines on 380 catchments, *J. Hydrol.*, 517, 1166-1175,  
1248 <https://doi.org/10.1016/j.jhydrol.2014.04.059>, 2014a.  
1249  
1250 Valéry, A., Andréassian, V., and Perrin, C.: ‘As simple as possible but not simpler’: What  
1251 is useful in a temperature-based snow-accounting routine? Part 2–Sensitivity analysis of  
1252 the Cemaneige snow accounting routine on 380 catchments, *J. Hydrol.*, 517, 1176-1187,  
1253 <https://doi.org/10.1016/j.jhydrol.2014.04.058>, 2014b.  
1254

1255 Viau, A. E. and Gajewski, K.: Reconstructing millennial-scale, regional paleoclimates of  
1256 boreal Canada during the Holocene, *J. Clim.*, 22, 316-330,  
1257 <https://doi.org/10.1175/2008JCLI2342.1>, 2009.  
1258  
1259 Zang, C. and Biondi, F.: treeclim: an R package for the numerical calibration of proxy-  
1260 climate relationships, *Ecography*, 38, 431-436, [10.1111/ecog.01335](https://doi.org/10.1111/ecog.01335), 2015.  
1261  
1262 Zhang, X., Harvey, K. D., Hogg, W., and Yuzyk, T. R.: Trends in Canadian streamflow,  
1263 *Water Resour. Res.*, 37, 987-998, <https://doi.org/10.1029/2000WR900357>, 2001.  
1264  
1265 Zolitschka, B., Francus, P., Ojala, A. E., and Schimmelmann, A.: Varves in lake  
1266 sediments—a review, *Quaternary. Sci. Rev.*, 117, 1-41,  
1267 <https://doi.org/10.1016/j.quascirev.2015.03.019>, 2015.